修士学位論文

Accumulation and manipulation of positrons, and synthesis of antihydrogen atoms

陽電子の蓄積・制御と反水素合成

東京大学大学院理学系研究科
物理学専攻
学籍番号 35096039
金燦鉉

January 06, 2011

Contents

Chapter 1

Introduction

1.1 CPT theorem

The CPT theorem or the CPT-symmetry is considered as one of the most fundamental principles of physics laws in our universe. It states that local Lorentz-covariant quantum field theory is invariant under the CPT operation, which consists of charge conjugation (C), space inversion (P), time reversal (T). As consequences of the CPT theorem, following propositions are derived.

- A particle and its counterpart antiparticle have the same mass
- A particle and its antiparticle have magnetic moments of the opposite sign and the same magnitude
- A particle and its antiparticle have the same life time

According to the big bang theory of the origin of the universe, equal amounts of matter and antimatter should have been formed. If the CPT theorem is the fundamental principle of the nature, there should still be a lot of observable antimatter as large as matter. However, it is seemed that this prospect is not consistent with empirical evidence which imply the quantity of matter is much larger than that of antimatter in our universe. This is one of the important motivations which demand the investigation of the CPT-symmetry.

It has been revealed experimentally that the P-symmetry and the CP-symmetry are violated. To test the CPT-symmetry, various experiments using particle-antiparticle pairs (e^-–e^+, p–$\overline{p}$, μ^+–μ^-, etc.) have been executed. (see Fig. 1.1) The most accurate test of the CPT-symmetry until now has been done by comparing the decay process of K^0 and $\overline{K^0}$ [1].

$\frac{(m_{e^-}-m_{e^+})}{m}$	$< 8 \times 10^{-9}$
$\frac{(m_p-m_{\overline{p}})}{m}$	$< 2 \times 10^{-9}$
$\frac{(q_{e^-}-q_{e^+})}{q}$	$< 4 \times 10^{-8}$
$\frac{(q_p-q_{\overline{p}})}{q}$	$< 2 \times 10^{-9}$
$\frac{(g_{e^-}-g_{e^+})}{g}$	$(-0.5 \pm 2.1) \times 10^{-12}$
$\frac{(g_p-g_{\overline{p}})}{g}$	$(-2.4 \pm 2.9) \times 10^{-5}$
$\frac{(g_{\mu^+}-g_{\mu^-})}{g}$	$(2 \pm 8) \times 10^{-5}$
$\frac{(\tau_{\mu_+}-\tau_{\mu_-})}{\tau}$	$(2.6 \pm 1.6) \times 10^{-8}$
$\frac{(m_{K^0}-m_{\overline{K^0}})}{m}$	10×10^{-18}
$\frac{(\Gamma_{K^0}-\Gamma_{\overline{K^0}})}{m}$	$(8 \pm 8) \times 10^{-18}$

Table 1.1: Comparison of the particle and its antiparticle [2]

Antihydrogen is considered as the persuasive candidate to pass over this record. Since its CPT conjugate system, hydrogen, is the most accurately studied atomic system, an antihydrogen atom has a possibility to provide the most stringent test of the CPT-symmetry. [3,4]

	experiments [Hz]	$\frac{\Delta\nu_{exp}}{\nu}$	$\frac{\nu_{th}-\nu_{exp}}{\nu}$
ν_{1s-2s}	2,466,061,413,187,103(46)	1.7×10^{-14}	1×10^{-11}
ν_{HF}	1,420,405,751.7667(9)	7.0×10^{-13}	$(3.5 \pm 0.9) \times 10^{-6}$

Table 1.2: Spetroscopic precision of hydrogen atom

1.2 The measurement of the ground-state hyperfine splitting

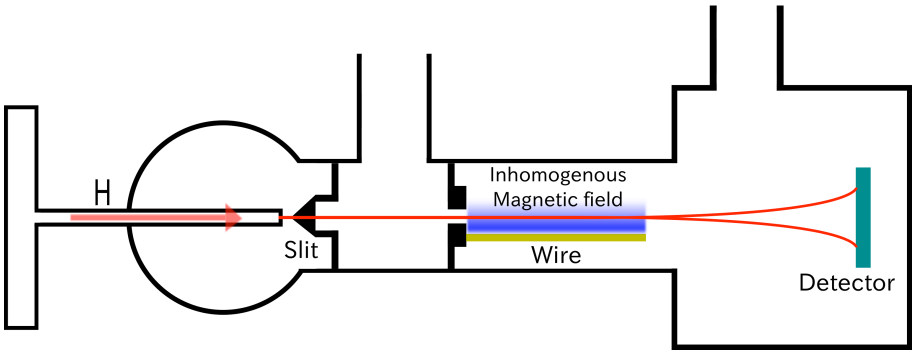

Figure 1.1: Rabi's experiment

The measurement of the ground-state hyperfine splitting (GS-HFS) frequency ν_{HF} in hydrogen has been improved since 1930 s. Rabi and his colleagues [5,6] designed the Stern-Gerlach type arrangement as shown in Fig. 1.1. Anthiydrogen atoms passing through the slit are injected in a region with inhomogeneous magnetic fields produced by electric currents. Then trajectories of hydrogens are changed depending on the magnetic moment of hydrogen atoms. From the distance of splitted hydrogen beam, they earned the value $\nu_{HF} = 1421.3 \pm 0.2\ MHz$. After Nafe and Nelson [7] improved the experiment by applying magnetic resonance, Prodell and Kusch [8] reached $\nu_{HF} = 1420.4051 \pm 0.0002\ MHz$. This precision is higher than the prediction of theory.

Using a microwave cavity in a similar way, we are planning to measure the ground-state hyperfine splitting of antihydrogen atoms. Figure 1.2 shows a conceptual setup of the experiment. Antihydrogen atoms synthesized in an apparatus called Cusp trap are extracted by a cusp magnetic field and focused to the microwave cavity. When antihydrogen atoms are ejected from Cusp trap, they are spin-polarized in the low field seeking state. If the frequency applied in the cavity matches with ν_{HF}, their spins are reversed to high field seeking states. In this state, when antihydrogen beam passes through the sextupole magnet, they diverge so that the counts of $\overline{H}$ detector decrease. On the contrary to this, if the frequency of the cavity does not correspond to ν_{HF}, antihydrogen beam is focused to the detector and signal count increases. Consequently, we can measure ν_{HF} by observing the antihydrogen number as a function of the frequency of the microwave cavity. Comparison of the

ν_{HF} values between hydrogen and antihydrogen is our final goal to the CPT theorem.

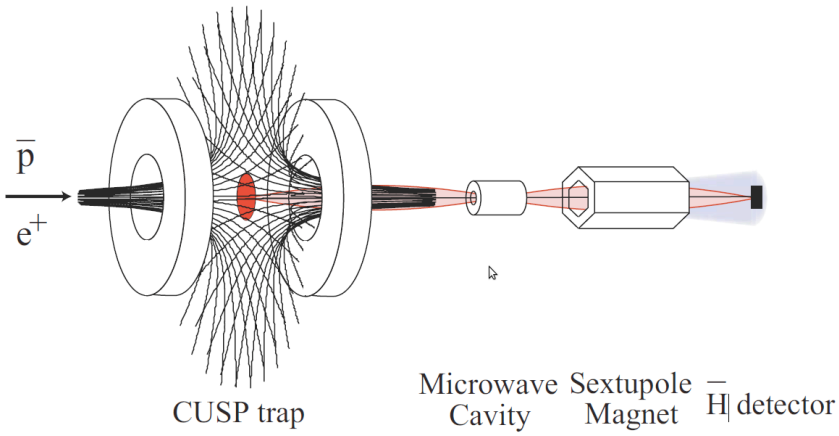

Figure 1.2: A concetual setup for the measurement of ground-state hyperfine transition of antihydrogen atoms.

1.3 Antihydrogen

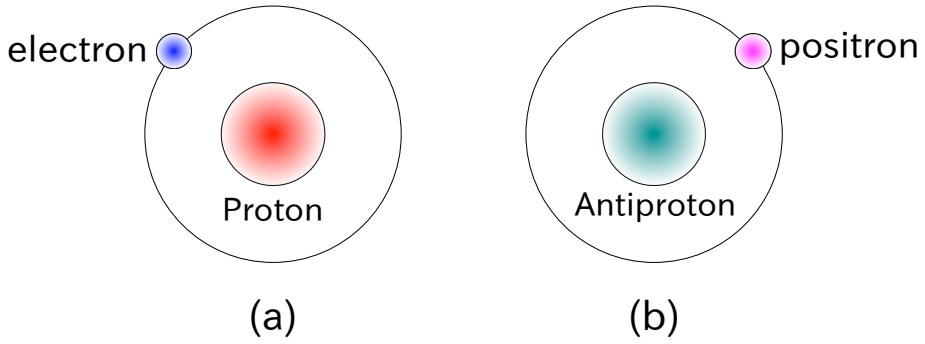

Figure 1.3: (a) Hydrogen and (b) antihydrogen

Antihydrogen is the antimatter counterpart of hydrogen. An antihydrogen atom is composed of a negatively charged antiroton and a positively charged positron, which are respectively the antiparticles of a proton and an electron (see Fig. 1.3). To synthesize antihydrogen atoms, the following recombination processes are considered as main reactions.

(1) Radiative recombination [9]

$$\overline{p} + e^+ \rightarrow \overline{H}(n,l) + h\nu \tag{1.1}$$

The reaction rate Γ_r [10] is given by

$$\Gamma_r = \frac{N_{\overline{p}} N_{e^+} \sigma_r \nu}{V} \propto \sqrt{\frac{1}{T}}\,, \tag{1.2}$$

where $N_{\overline{p}}$ and N_{e^+} are respecively the numbers of antiprotons and positrons, which are confined in a volume V at temperature T. ν is their relative collision velocity.

(2) Three body recombination [11]

$$\overline{p} + e^+ + e^+ \rightarrow \overline{H}(n,l) + e^+ \tag{1.3}$$

The reaction rate Γ_t is given by

$$\Gamma_t \propto \left(\frac{N_{e^+}}{V}\right)^2 \left(\frac{1}{T}\right)^{\frac{9}{2}}\,. \tag{1.4}$$

As described above, the energy of an antiproton and a positron is released as a photon in the radiative recombination process. In the three body recombination process, one antiproton and two positrons participate in the reaction. One positron and the antiproton form antihydrogen while another positron takes away the excess energy. If the positron cloud is cold and has a high density, it is noted that theoretically three body recombination dominates in the case as seen in equations 1.2 and 1.4.

The first observation of antihydrogen was reported from CERN in 1996 [12], and Fermilab in 1998 [13]. In 2002, two international collaborations at CERN, ATHENA [14] and ATRAP [15], succeeded in producing a large number of antihydrogen atoms. They used a so-called nested potential configuration for mixing antiprotons and positrons (See Fig. 1.4).

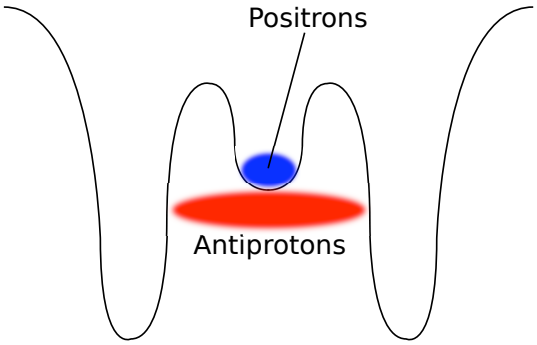

Figure 1.4: Nested potential is designed for trapping positrons and antiprotons simultaneously. Positrons are confined in the small well at the center while antiprotons are confined in the outer well.

The nested potential is generated by applying voltages to separated ring electrodes which are axially symmetric. By overlapping a magnetic field with this nested potential, antiprotons and positrons can be trapped 3-dimensionally. A brief procedure for mixing them follows the next few steps. First, there are previously trapped positrons in the well at the center and cooled down to room temperature. Second, antiprotons are injected into the nested potential and lose their energy colliding with positrons repetitively. Third, heated positrons lose their energy by synchrotron radiation. As a consequence, the relative velocity of antiprotons and positrons decrease and antihydrogen atoms are eventually formed through this procedure.

1.4 Experimental apparatus

1.4.1 Cusp trap

Cusp trap is an apparatus for antihydrogen synthesis. It is designed to trap antiprotons and positrons simultaneously and mix them. Since both antiproton and positron have electric charge, they can be captured 3-dimensionally by superimposing electric and magnetic fields.

Figure 1.5 shows a cross-sectional view of Cusp trap. As is seen, a multi ring electrode (MRE) is situated in a bore of superconducting magnet. The MRE of Cusp trap consists of 17 cylindrical copper rings. U4 and D4 are devided into four respectively. (See Fig. 1.6 and Fig. 1.7) By applying a DC voltage to each channel of the MRE, electric potential is generated or manipulated depending on the situation. Meanwhile, magnetic fields are provided by a superconducting anti-Helmholtz coil having axial symmetry. An anti-Helmholtz coil is a pair of solenoids in which currents flow in opposite directions. This produces inhomogenenious cusp magnetic fields (2.7 T) which is a key to extract an antihydrogen beam.

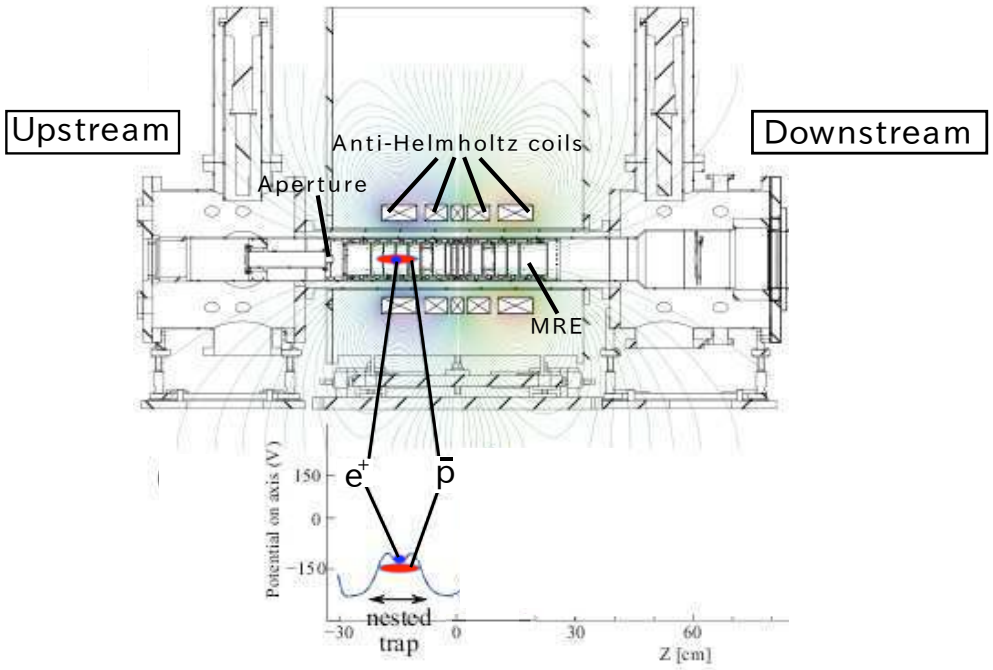

Figure 1.5: A cross-sectional view of Cusp trap and a nested potential configuration along the axis

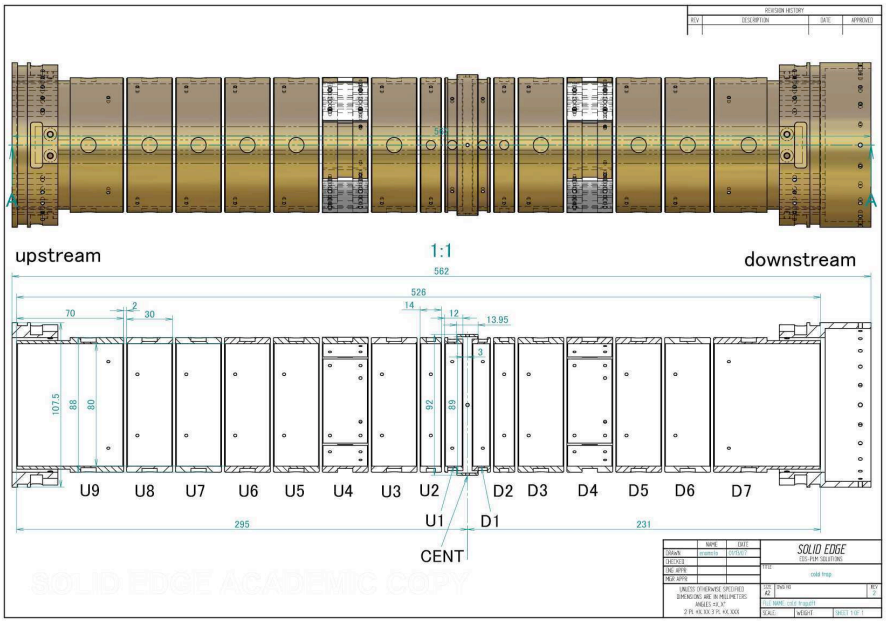

Figure 1.6: MRE of Cusp trap

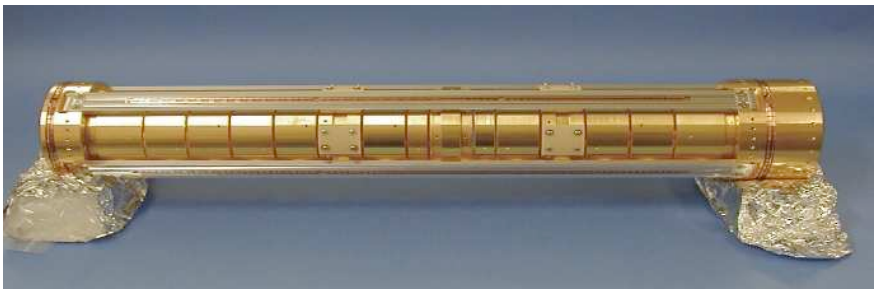

Figure 1.7: A photo of MRE of Cusp trap

1.4.2 Antiproton decelerator (AD) and antiproton trap

Antiprotons are provided by the antiproton decelerater (AD) at CERN (European Organization for Nuclear Research), Geneva, Switzreland. Figure 1.8 schematically shows the accelerator complex including AD.

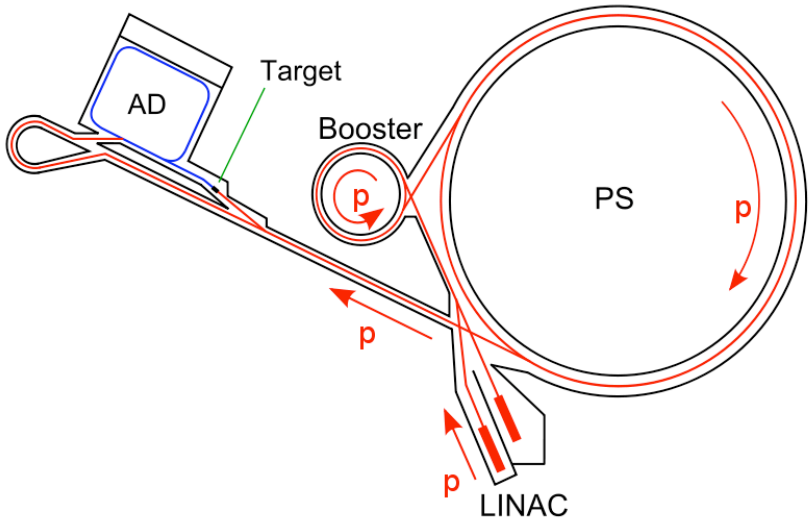

Figure 1.8: A diagram of PS-complex at CERN

Below are the details of producing and decelerating antiprotons.

1. A pulsed 26 GeV/c proton beam is provided from PS (Proton synchrotron) as a pulsed beam.

2. The proton beam hits the iridium target installed in front of the AD and antiprotons are produced by following pair production process,

$$p + p \rightarrow p + p + p + \overline{p}. \tag{1.5}$$

3. 3.5 GeV/c antiprotons are collected by a magnetic horn and injected into AD.

4. Antiprotons are cooled and decelerated to 100 MeV/c (5.3 MeV) by stochastic cooling and electron cooling.

5. Antiprotons are ejected into the experimental area. About 2×10^7 antiprotons per 90 s are supplied as a 100 ns length beam. (See Fig. 1.9)

Antiprotons decelerated by AD are delivered to each experiment, as is seen in Fig. 1.9. In the AD facility, there are three running experiments ALPHA, ATRAP and ASACUSA, aiming to synthesize antihydrogen atoms. Our group belongs to ASACUSA (Atomic Spectroscopy And Collisions Using Antiprotons). All apparatus used in this experiment are located in the ASACUSA area.

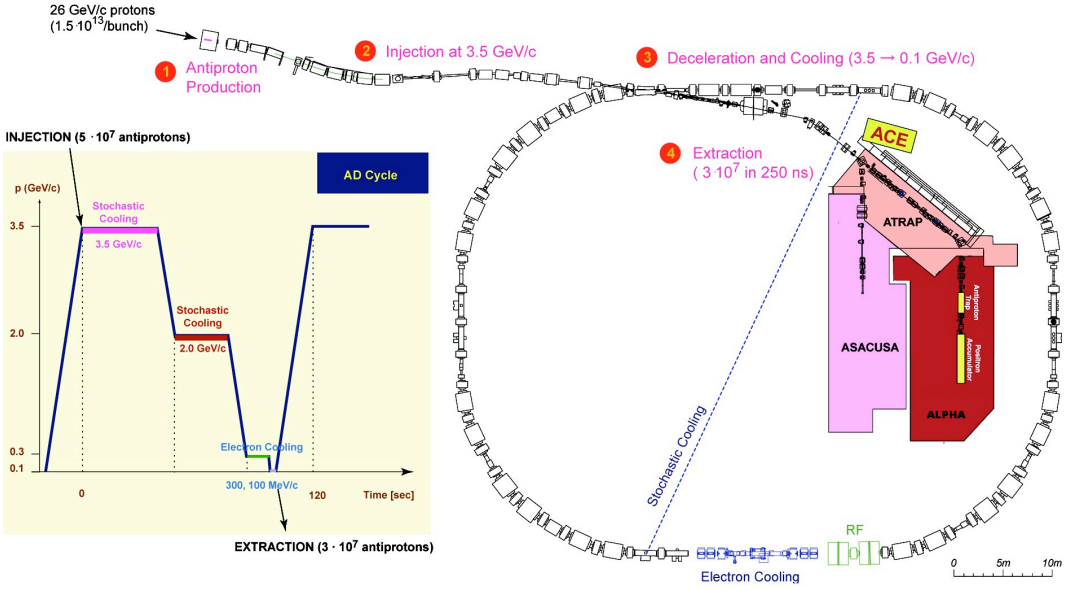

Figure 1.9: Brief diagrams of operation procedure (left bottom) and the experiment area of AD

The 5.3 MeV antiprotons from AD are necessarily decelerated furthermore to be trapped. To reduce the energy efficiently, ASACUSA uses Radio frequency quadrupole decelerator (RFQD), which is used in reversed direction of a usual RFQ linear accelerator. The antiprotons are decelerated to 100 keV by RFQD with 30% efficiency and injected into a degrader foil positioned in front of the antiproton trap. Compared with other experimets in which antiprotons are directly injected into the degrader foils, RFQD allows the foil much thinner and loss of antiprotons decrease. Antiprotons passing through the degrader foil are injected into the MRE of the antiproton trap. Being mixed with the preloaded electrons in the antiproton trap, they lose their energy by Coulomb scattering and are cooled down to the evironment temperature [16]. The typical number of the antiprotons captured per one AD shot was about $7 \sim 8 \times 10^5$.

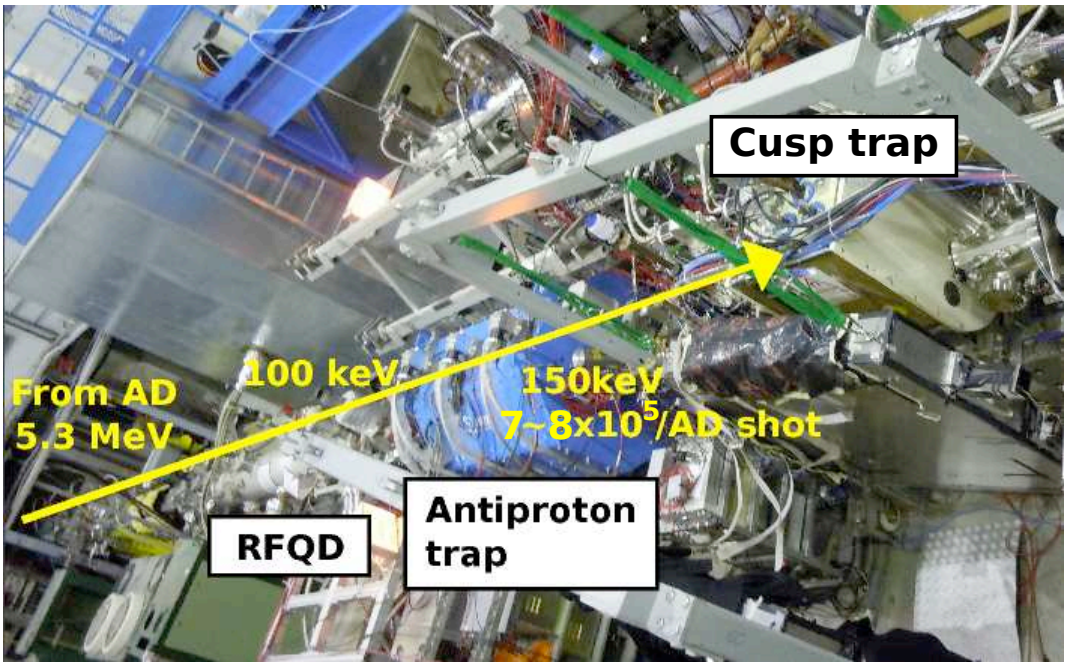

Figure 1.10: A photo of ASACUSA beam line

1.5 Aim of the experiment

A goal of this experiment is to synthesize antihydrogens for the hyperfine structure measurement. As ingredients of antihydrogen atoms, antiprotons and positrons are respectively pre-accumulated in the antiproton trap and the positron accumulator before mixed in Cusp trap. Schematic descriptions about the antiproton trap and Cusp trap are already mentioned. In this paper, accumulation and manipulation of positrons will be mainly discussed as a part of the experiment for synthesizing antihydrogens. Below are three main aims of this study:

1. Accumulating positrons in the positron accumulator with high efficiency (Chapter 2),

2. Transporting positrons as a pulsed beam from the positron accumulator to Cusp trap (Chapter 3),

3. Manipulating positrons to synthesize a large number of antihydrogen atoms in Cusp trap (Chapter 4).

Figure 1.11 shows a schematic view of the experimental arrangement. Details will be depicted in the following chapters in order, from upstream to downstream.

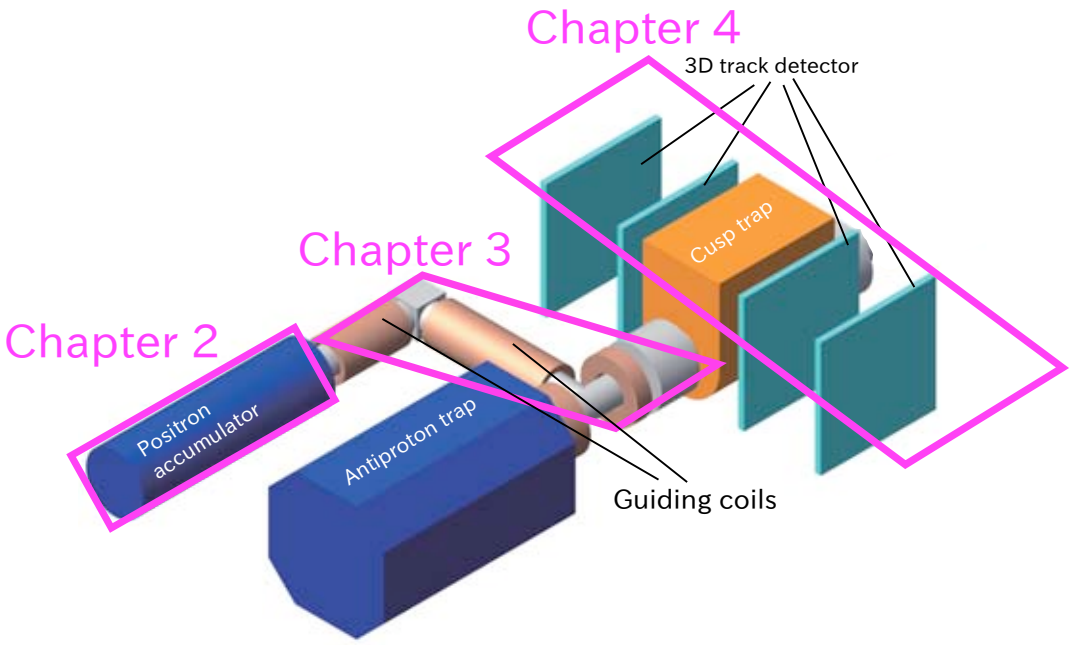

Figure 1.11: A schematic view of the experimental arrangement

Chapter 2

Positron Accumulation

2.1 Basic conception and prerequisites of the positron accumulator

Before a detailed description of the apparatus for accumulating positrons, a basic conception and required conditions of the design will be discussed in this section.

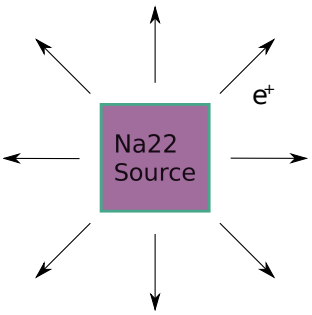

Figure 2.1: Positrons are ejected isotropically from radioactive source

Firstly, what we need to think is the selection of a positron source. ^{22}Na, known as the most popular positron source, is selected. Contrary to the case of AD supplying antiprotons, this source does not provide positrons as the form of a pulsed beam. As Fig. 2.1 shows, positrons are emitted isotropically from the source with broad energy distribution. Additionally, positrons annihilate when they interact with matters. Therefore, the system for accumulating a large amount of positrons must satisfy the following prerequisites.

(1) guiding positrons to the specific direction and focus them

(2) reducing positron energy for capturing

(3) confining positrons 3-dimensionally in a fixed region

(4) being operated in high vaccum condition against positron annihilation

The items (1) and (3) are intimately related tasks. In a strong magnetic field, positrons are enforced to move along magnetic field lines and lose their transverse energy by synchrotron radiation. In the axial direction, they can be confined by an electric potential overlapped by the magnetic field. An assembly of multiple cylindrical ring electrodes and a superconducting solenoid provide proper electromagnetic fields for the confinement.

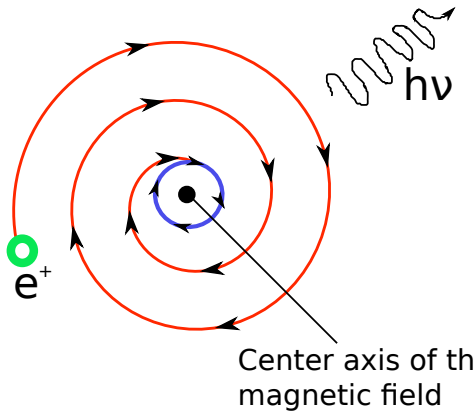

Figure 2.2: Synchrotron radiation. Magnetic field is coming out of paper.

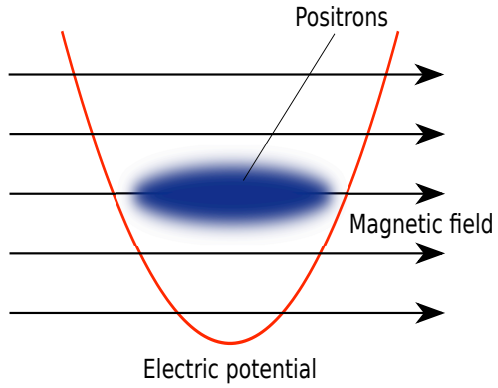

Figure 2.3: Confinment of positrons by electromagnetic field

To reduce the kinectic energy of positrons (3), several techniques have been developed [17,18]. Among them, the buffer gas method [17] is the most efficient technique for stopping and accumulating positrons until now. This method is also adopted for our experiment although a gas flow decreases the life time of positrons in the apparatus (4). Details of this method will be described in the following section.

2.2 Buffer gas method

The buffer gas method is widely used in various projects using positron beams. Two other experiments working on antihydrogen synthesis are adopt this scheme. It consists of a coupole of steps when they positrons are being captured through the accumulation process. Figure 2.4 is a brief diagram of the scheme.

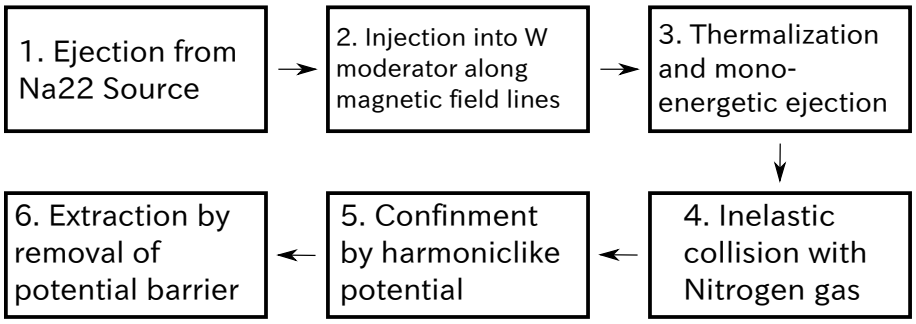

Figure 2.4: A brief scheme of the buffer gas method

The key points of this method are step 3 and 4 in the diagram. In order to stop positrons through collisions with gas molecules, they should be in a specific energy range for the reaction called electronic excitation dominates over other reaction channels which reduce usable positrons. For this reason, the material having negative work-function is used as a moderator to make positrons monoenergetic. The incident positrons become thermalized and are ejected with a narrow energy distribution. Two moderators are prepared in the present setup, one for the transmission and the other for the reflection. Transmission moderator emits moderated positrons to the same direction as the incident positrons. On the other hand, the reflective moderator reverse the direction of movement. (See Fig. 2.5) As described in Fig. 2.6, the emitted positrons from moderators collide with gas molecules and lose their energy again. Then some of them are guided by potential slope and trapped into the harmoniclike potential.

One problem of this method is the residual gas of the transportation line. Because in the present setup, we need to maintain the whole beamline in ultra high vaccum otherwise residual gas shortens the lifetime of antiparticles in Cusp trap. We separate positron accumulator and other apparatus' spacially by the gate valves. These gate valves are opened for few seconds when positrons are transported.

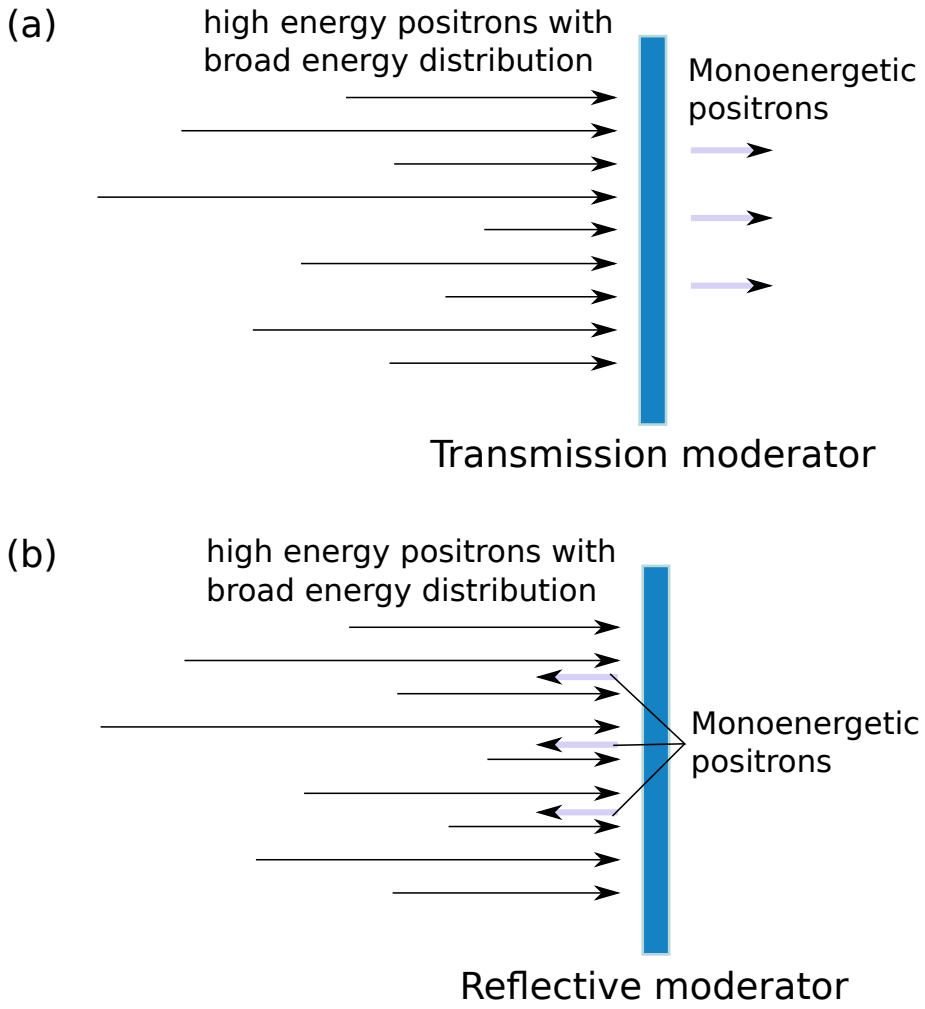

Figure 2.5: Positrons slowed down by (a) transmission moderator and (b) reflective moderator are ejected monoenergically

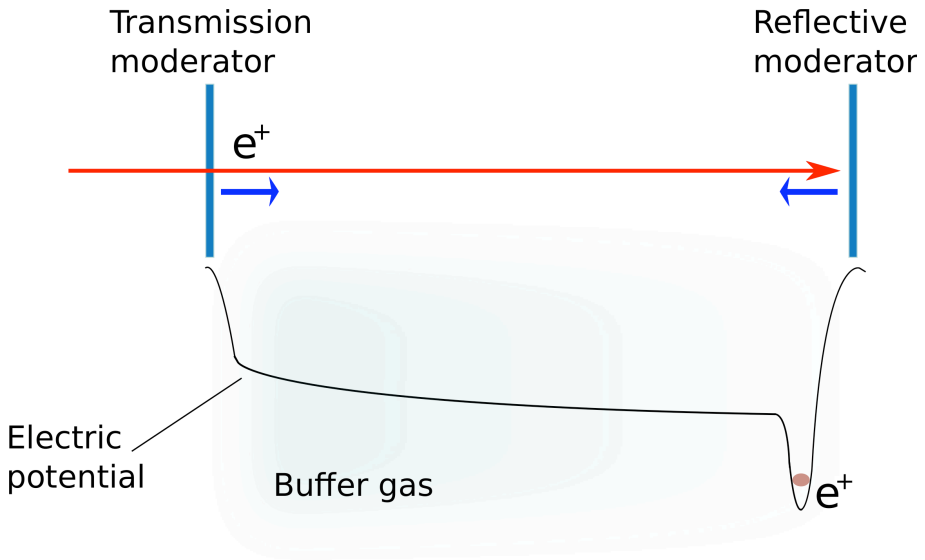

Figure 2.6: Positrons re-emitted from moderators are collinding with gas molecules. Some of them are trapped by harmoniclike potential which is located in the right side of the diagram

2.2.1 Selection of buffer gas

N_2 gas is used as buffer gas to stopping positrons. The subsection will reviews the experiment [19,20] which implies important information of interaction between positrons and diatomic gas. Colliding with diatomic molecules, following reactoins can occur:

direct ionization

$$AB + e^+ \rightarrow AB^+ + e^+ + e^-; \tag{2.1}$$

positronium formation

$$AB + e^+ \rightarrow AB^+ + Ps; \tag{2.2}$$

electronic excitaiton

$$AB + e^+ \rightarrow AB^* + e^+ \tag{2.3}$$

dissociation

$$AB + e^+ \rightarrow A + B + e^+; \tag{2.4}$$

direct annihilation

$$AB + e^+ \rightarrow AB^+ + 2\gamma; \tag{2.5}$$

Let us consider firtst three and skip others since cross sections of dissociation and direct annihilation are of orders of magnitude smaller than them [21].

Electronic excitaions can reduce the kinetic energy of positron without producing ions. Charge of ions expand positron cloud and increase the possibility that some positrons annihilate by collision with inner wall of the apparatus. For this reason, direct ionization decreases the accumulation efficiency of positrons. Positronium formation is also an obstruction. If positrons form positroniums by the combination with electrons, they cannot be trapped since positroniums are electrically neutral. Consequentely, in these three reactions, only electronic excitation contributes to stopping positrons.

It is noted that threshold of direct ionization is almost double of electronic excitation and positronium formation for some cases desribed in Table 2.1. If positron energy is lower than 10 eV, direct ionization can be neglected. In these cases, all we need to consider is the rate of the cross sections of electron excitation and positronium formation.

Diatomic Molecule	Electronic excitation	Positronium formation	Direct ionization
N_2	8.59eV	8.78eV	15.58eV
CO	8.07eV	7.21eV	14.01eV
O_2	7.05eV	5.4eV	12.2eV

Table 2.1: Threshold energy for each process of N_2, CO, O_2. Only in the case of N_2, the threshold of electronic excitation is smaller than that of positronium formation

Figure 2.7 shows the cross sections of electronic excitation and positron formation in N_2 and CO. In this graph, it is noted that N_2 molecules have the energy region from 8 eV to 11 eV where the cross section of electronic excitation is bigger than positron formation. Because the efficiency of stopping positrons increases when the rate of former cross section dominates, N_2 is more suitable as a buffer gas for accumulating positrons.

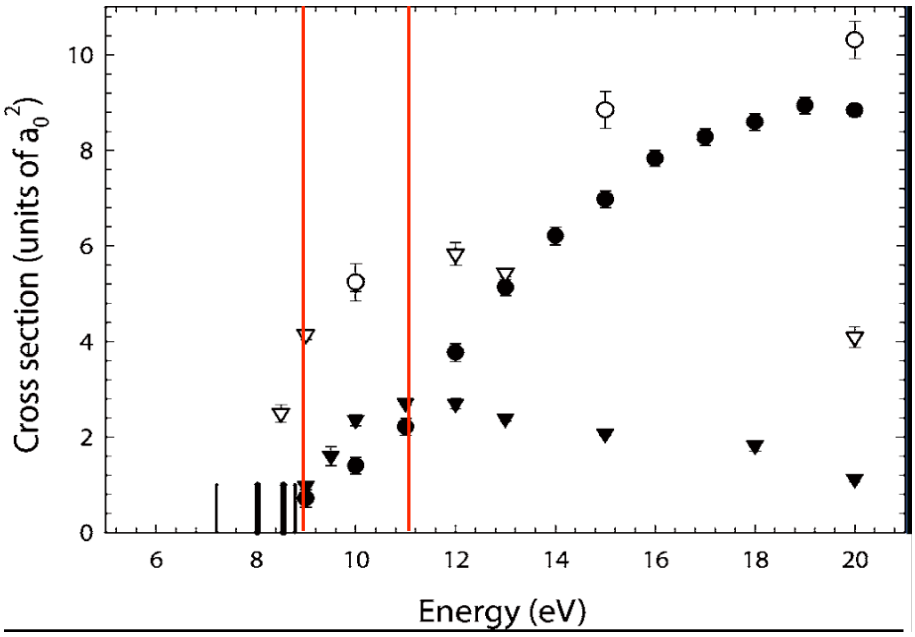

Figure 2.7: Cross sections of electronic excitation (inverted triangle) and positronium formation (circle) in N_2 (black) and CO (white). In the case of N_2, the cross section of electron excitation is larger than that of positronium formation in the energy region between the red lines.

2.3 Positron accumulator

In this section, we will describe the each component of the positron accumulator. Figure 2.8 shows a schematic view of the whole apparatus. As is seen in this figure, the ^{22}Na source, a buffer gas cell and the trap are equipped in the bore and surrounded by a superconducting solnenoid.

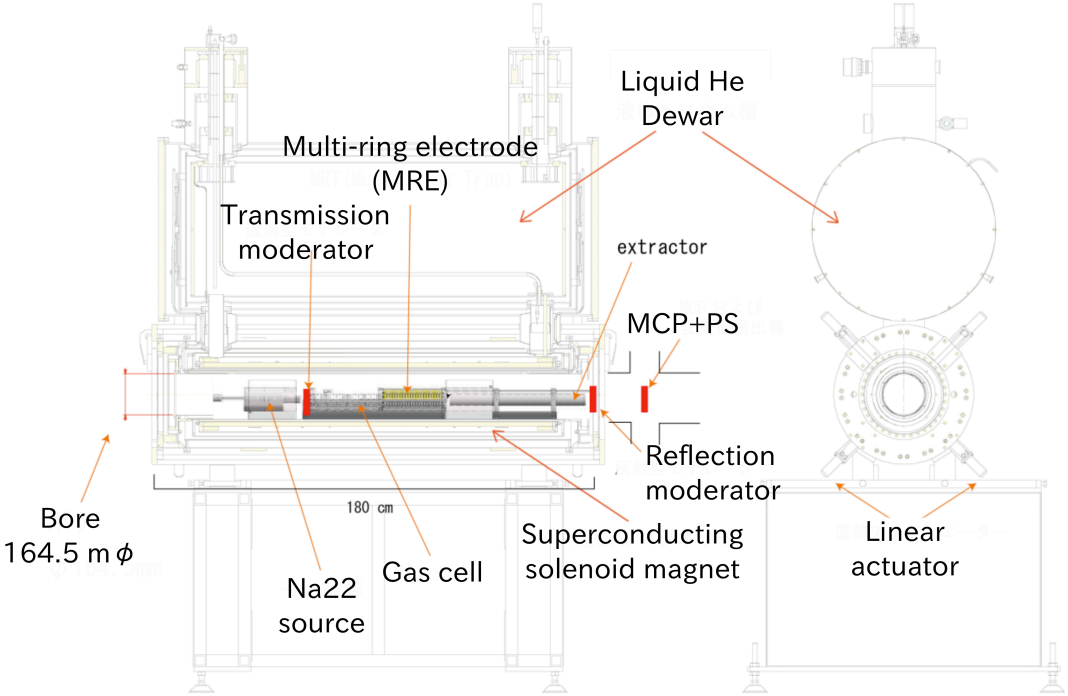

Figure 2.8: A schematic view of the whole set of positron accumulator

2.3.1 Supeconducting solenoid magnet

The magnetic field for trapping antiparticles is provided by a superconducting solenoid magnet. A cross sectional view of the magnet is drawn in 2.8. The specifications are summarized in Table 2.2

Designed maximum central magnetic field	5 T
Current for full field iron shield	112 A
Homogeneity volume	10 mm$\phi\times$ 1100 mm
Magnet clear room temperature bore diameter	164. 5mm
Nominal inductance	100 H
Stored energy	0.63 MJ
Magnet maximum sweep voltage	80 V
Energisation time 0 to 112 A	150 s
De-energization time 112 to 0 A	159 s

Table 2.2: Specifications of a superconducting magnet solenoid

To keep the solenoid superconducting state, liquid helium is used to cool it down. As is seen in Fig. 2.8, liquid helium is contained in a dewar which is connencted to the loop nearby superconducting solenoid. It is also used for cooling the inner bore of the apparatus.

2.3.2 Radioactive source

^{22}Na is used as the radioactive source of positrons. The source with 50 mCi(1.85 Gbq) was installed into the apparatus in 2008. It decays with 2.6 year half-lifetime. Accordingly, the radioactivity in 2010 was about half level of 2008 in 2010 beamtime.

Figure 2.10 shows the capsule in which ^{22}Na source is contained in a capsule. As described in Fig. 2.9, the source is covered by heavy alloy shields which consist of 94% tungsten, 4% nickel and 2% copper. The addition of nickel and copper renders tungsten more machinable. Mechanical shutter made by W-alloy is installed in front of the entrance and opened only when the accumulation is in progress.

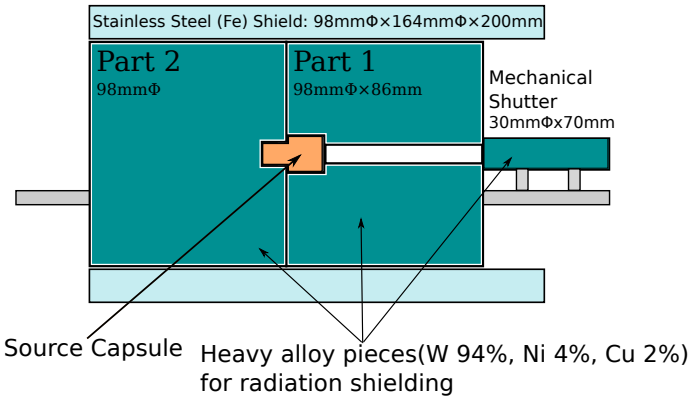

Figure 2.9: ^{22}Na source covering by heavy alloy radiation shields

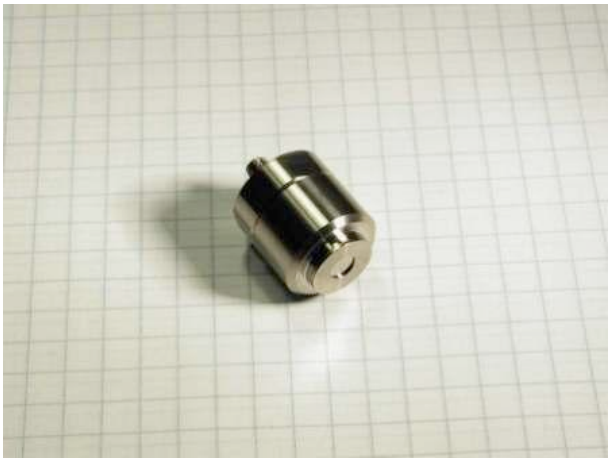

Figure 2.10: A photo of source capsule

2.3.3 Gas cell, Multi-ring electrode (MRE), and extractor (The trapping region)

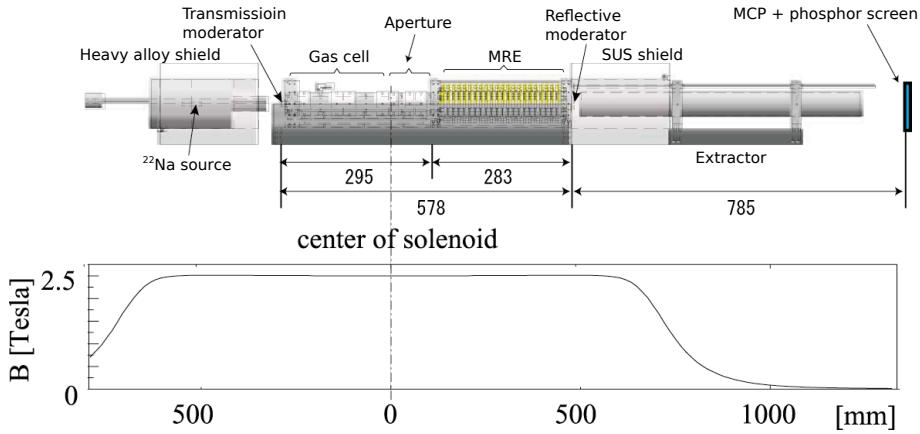

Figure 2.11: A diagram of the trapping region

Gas cell

Positrons re-emitted from the moderators lose their energy in the gas cell colliding with N_2 molecules. As shown in Fig. 2.12, a gas injection tube is close to the transmission moderator.

Multi-ring electrode (MRE)

Positrons losing their energies in the gas cell are accumulated in a trap, which is made of electrical potential overlapped with a magnetic field. The magnetic field is provided by the superconducting solenoid.

Multi-ring electrode (MRE) is used for providing the electrical potential that retains the longitudal motion of the positrons. It consists of 25 cylindrical gold-coated aluminum rings whose inner diameter is 42 mm. The neighboring two electrodes are separated by 1 mm. (See Fig. 2.13 and Fig. 2.14) This arrangement allows us to independently bias each electrode to yield various potential distributions.

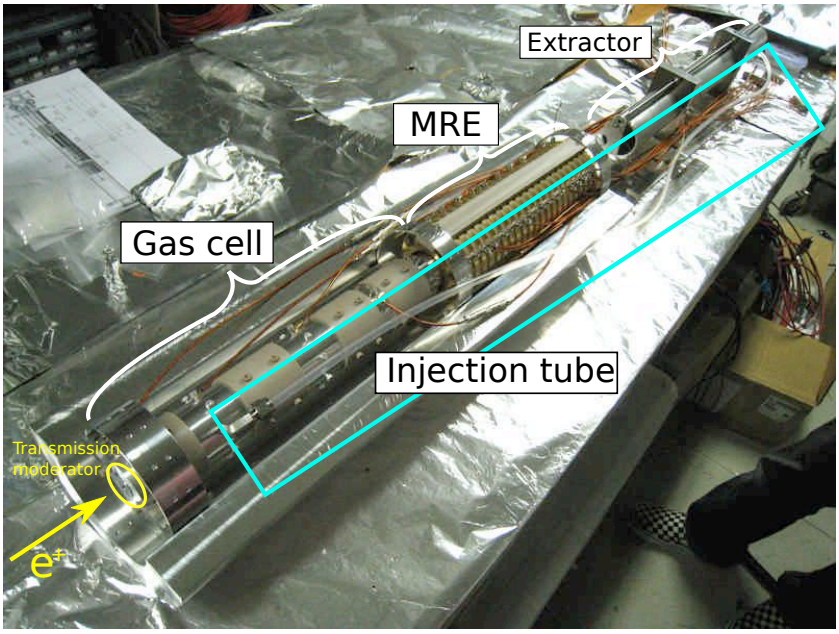

Figure 2.12: A photo of the trapping region

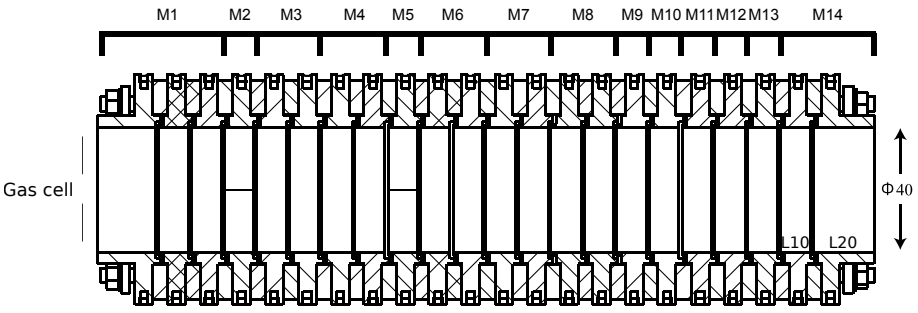

Figure 2.13: A cross-sectional view of MRE of the positron accumulator

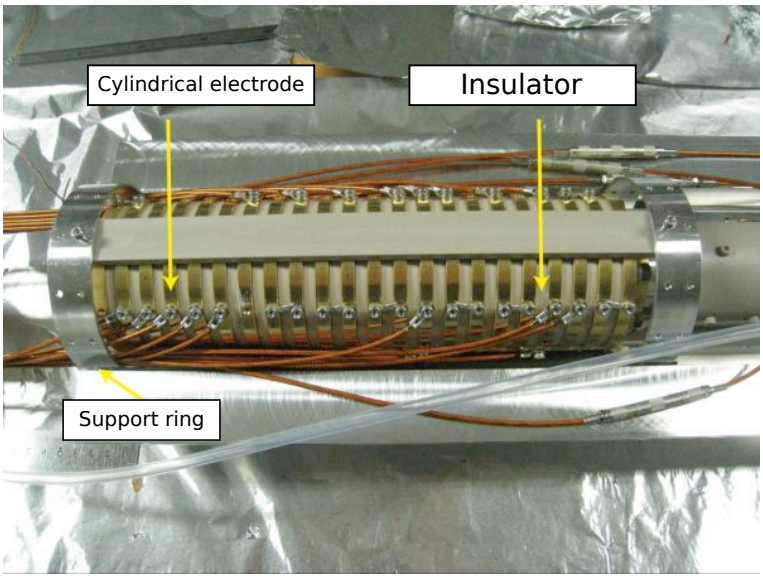

Figure 2.14: A photo of MRE of the positron accumulator

2.3.4 Moderator

The function of the moderator is to make positrons mono-energetic. Along magnetic field lines, some of the positrons emitted from the ^{22}Na source are guided to the direction of MRE. At this moment the positron energy is distributed continuously from 0 to 546 keV. To be captured, they should be monoenergetic and have low energy to interact with nitrogen molecules. Positrons injected to moderators are ejected with narrow energy spread about 75meV in room temperature. Then the energy level can be adjusted by potential manipulation.

Figure 2.15 and Figure 2.16 show the installation of transmission and reflective moderators. As described in Figure 2.11, the reflective moderator is positioned between MRE and extractor. It is equipped in the movable system, so it can be substituted by an aperture when positrons are extracted from the trapping region.

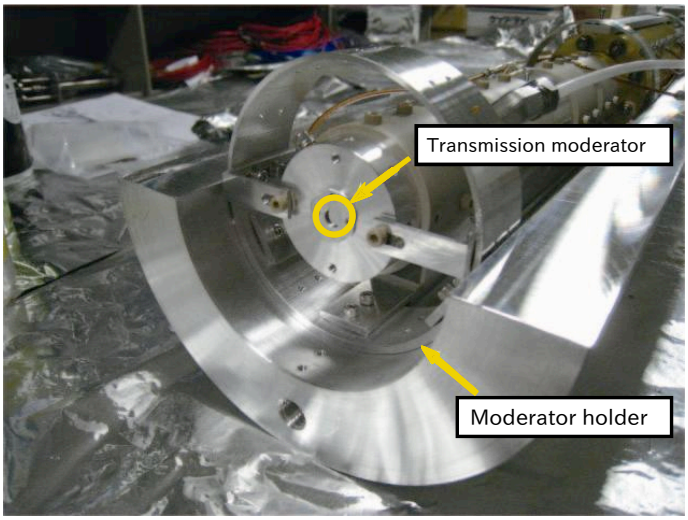

Figure 2.15: Transmission moderator adjoined by one side of the buffer gas cell

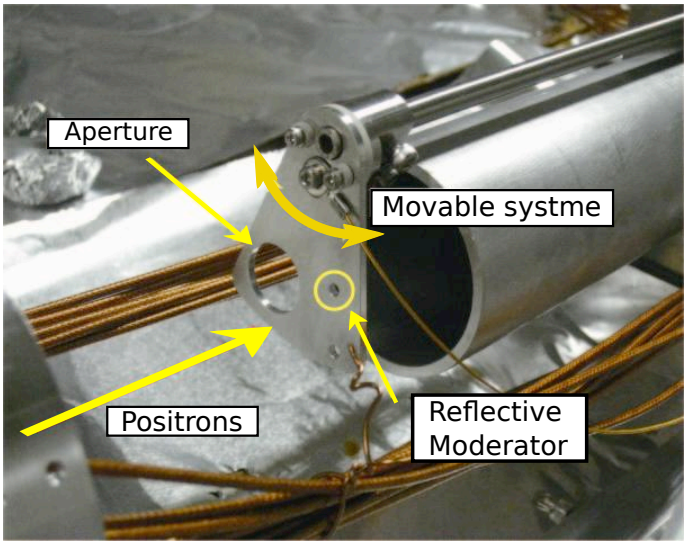

Figure 2.16: Reflective moderator and aparture in the movable system.

2.3.5 N_2 gas injection and evacuating system

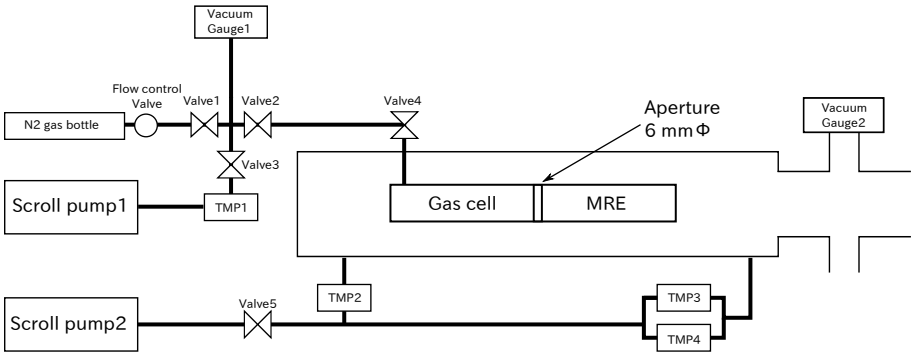

Figure 2.17: A diagram of evacuation system in the positron accumulator

Figure 2.17 shows a schematic drawing of the gas injection and evacuation system. It consists of a N_2 gas bottle, two scroll pumps, 4 turbo molecular pumps (TMP), 2 vacuum gauges, several tubes and valves connecting each part of the system. Nitrogen gas flows into the bore of the positron accumulator through the flow controle valve, valve 1, valve 2, and valve 4 while valve 3 is closed. Turbo molecular pumps TMP2, TMP3, and TMP4 and scroll pump 2 evacuate the inner bore. Since gas injection tube is connected to the side close to the source, a pressure gradient is generated through the gas cell. An aperture with 6 mm diameter is installed between the gas cell and MRE. This aperture obstructs the flow of nitrogen gas to keep the pressure in MRE is kept low. Consequently, this structure provides relatively low gas density in the MRE and the life time of trapped positrons increase. Two vacuum gauges are used to monitor pressures of the system. Gauge 1 is connected to the N_2 bottle side while gauge 2 is close to the bore of positron accumulator. The general pressure slope of the bore can be assumed by reading the values of these two gauges.

2.3.6 Monitor system

A combination of a micro-channel plate (MCP) and a phosphor screen is used as a monitor to measure the number and beam profile of positrons. (See Fig. 2.18) MCP is a planar component which consists of millions of tiny glass capillaries. Collided by positrons, the front surface of the MCP emits secondary electrons. By applying a potential difference between front and back of the MCP, the secondary electrons are accelerated to the back side. Then they strike the channel surface again, produce more secondary electrons, and so on. Consequently the numerous secondary electrons proportional to the number of incident positrons are ejected to the phosphor screen, which is positioned at the rear of the MCP.

The phosphor screen converts the electrons ejected from the MCP back into photons. For its luminosity, combining with the MCP allows us to provide the X-Y distribution of positrons. The profile of the positron beam can be taken by using a CCD camera.

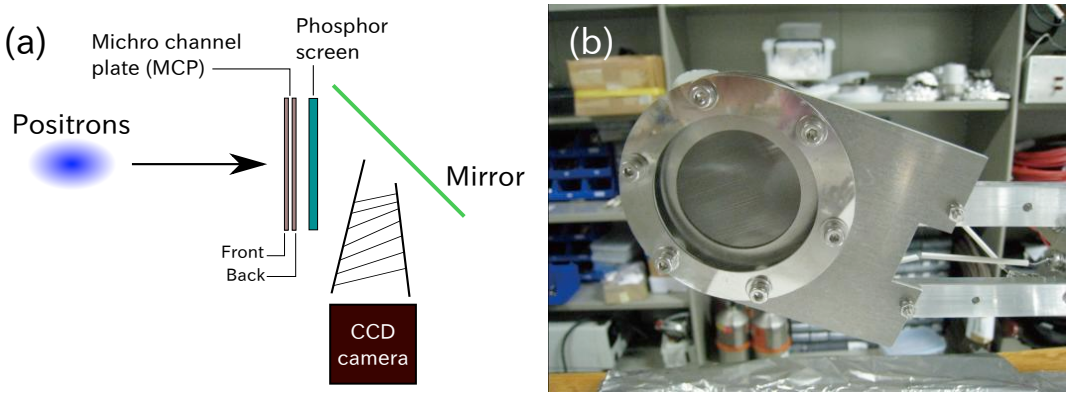

Figure 2.18: (a) A schematic view of the positron monitor which consists of a MCP, a phosphor screen, and a CCD camera (b) A photo of combined MCP and phosphor screen

Calibration of MCP

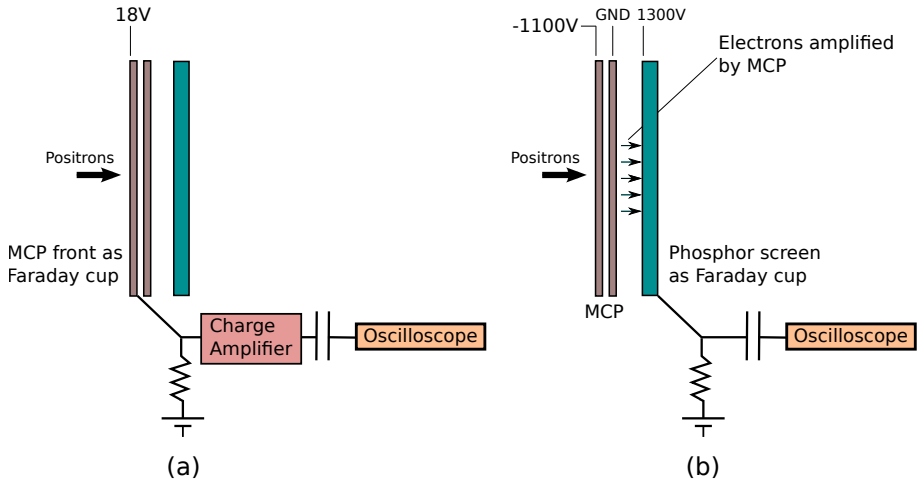

Figure 2.19: A schematic view of connection between MCP, PS and Oscilloscope.(a) Total charge of positrons can be measured directly by using the MCP front as Faraday cup. (b) Phosphor screen performs as Faraday cup used when MCP is used for amplification.

In our experimental setup, the most accurate way of counting the number of positrons is using the MCP front as a Faraday cup, connecting to an oscilloscope through charge amplifier as described in Fig. 2.19 (a). However, this method is not efficient when the number of positrons is smaller than 10^5 because the noise level is comparable with the signal from positrons. Therefore, as showns in Fig. 2.19 (b), the MCP is used to amplify the signal from positrons and the phosphor screen performs a Faraday cup until the accumulation efficiency becomes stable. Although the later method is mainly used for measuring the number of positrons before callibrating the amplificatoin rate by MCP, Let us use this amplification rate to express the quantity of positrons as the number of them.

Figure 2.20 shows the relation between suppresion voltage and the number of positrons. Suppression voltage is used to restrain the emission of secondary electrons from MCP front when positrons inject to the surface. From this figure, it seemed that secondary positrons are almost suppressed when applied volatage is more than 18 V.

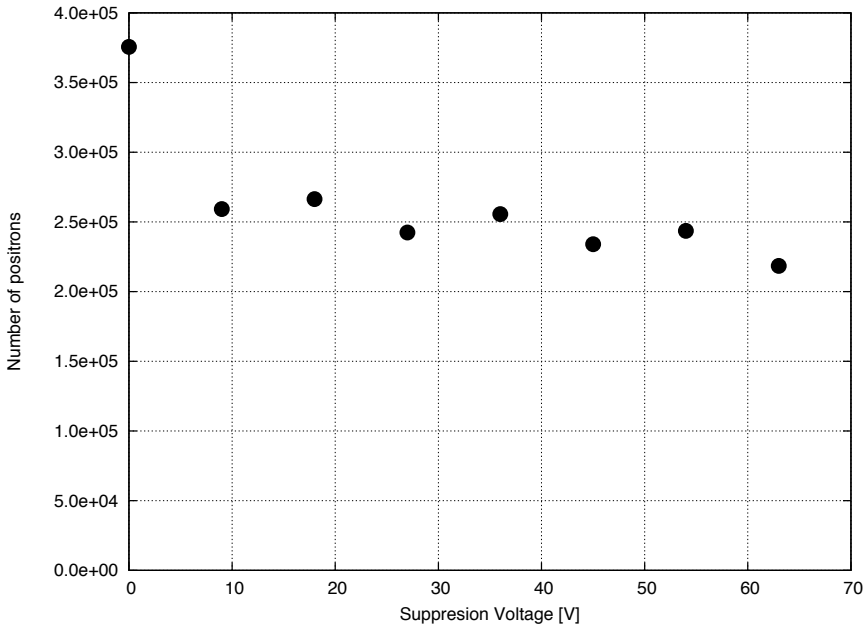

Figure 2.20: Suppresion volatage and the number of positrons measured by using MCP front as a Faraday cup

2.4 Process of accumulating positrons

Figure 2.21 shows the brief procedure of accumulating positrons.

(a) When the operation begins, the heavy alloy shutter of ^{22}Na source is open and positrons are guided to the trapping region. Then they are injected to the transmission moderator or the reflective moderator. Some of them are thermalized and re-emitted to the buffer gas region. Furthermore, some of these re-emitted positrons lose their energy by colliding with buffer gas molecules. the potential difference between the moderator and buffer gas cell is adjusted to the appropriate level where the electron excitation is dominant. Low energy positrons are guided by the smooth slope and accumulated to the accumulating well close to the exit of the trapping region.

(b) To extract the trapped positrons, the reflective moderator is removed from the axis. A combination of a MCP and a phosphor screen is injected to the axis. The heavy alloy shutter of the ^{22}Na source is closed.

(c) The trapped positrons are ejected by removing the potential barrier of the exit side. A pulsed positron beam is monitored.

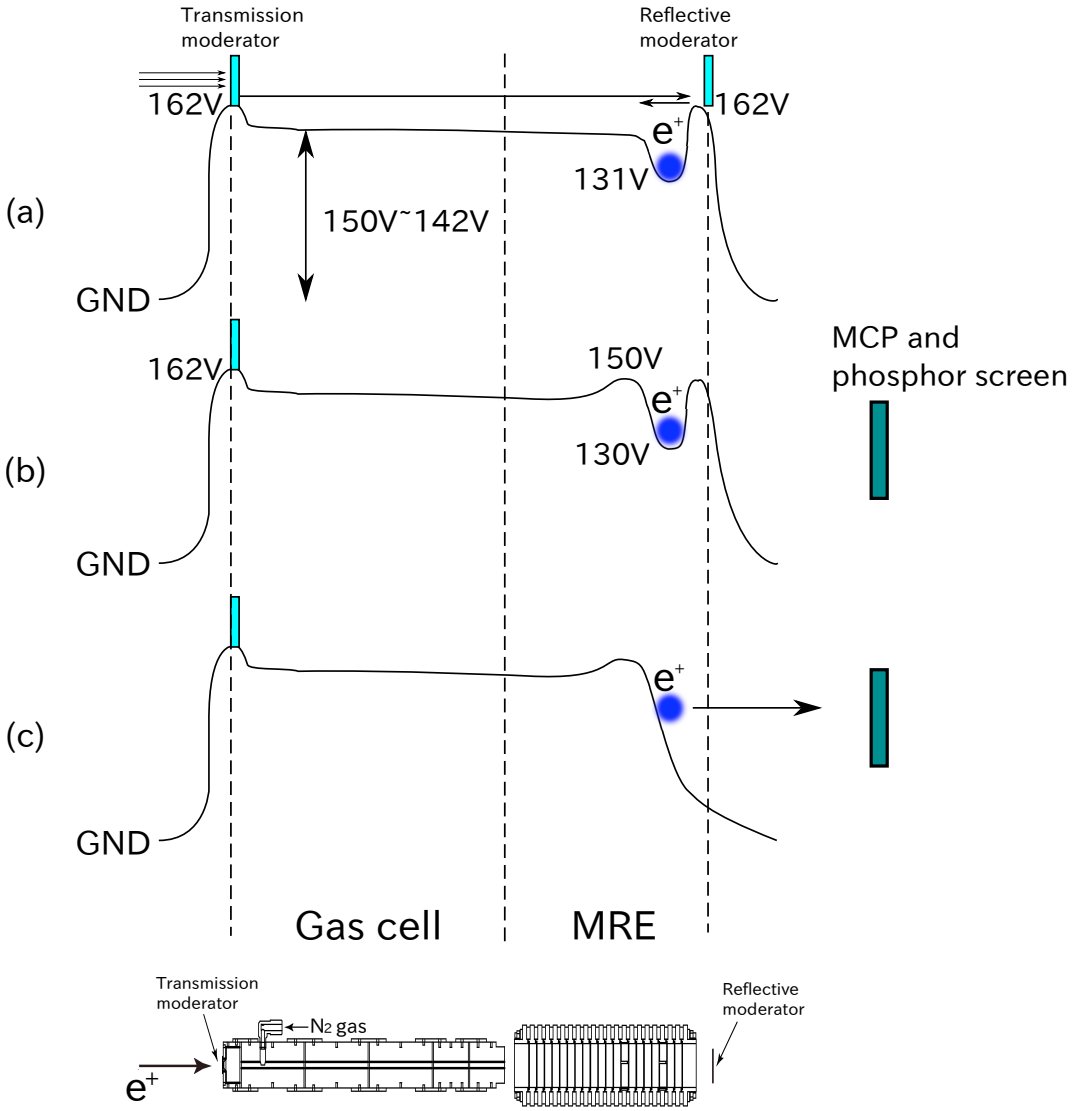

Figure 2.21: The procedure of accumulating positrons

2.5 Parameters

2.5.1 Magnetic field

As is seen in Fig. 2.22, the number of accumulated positrons increases when the magnetic field in the apparatus is strong.

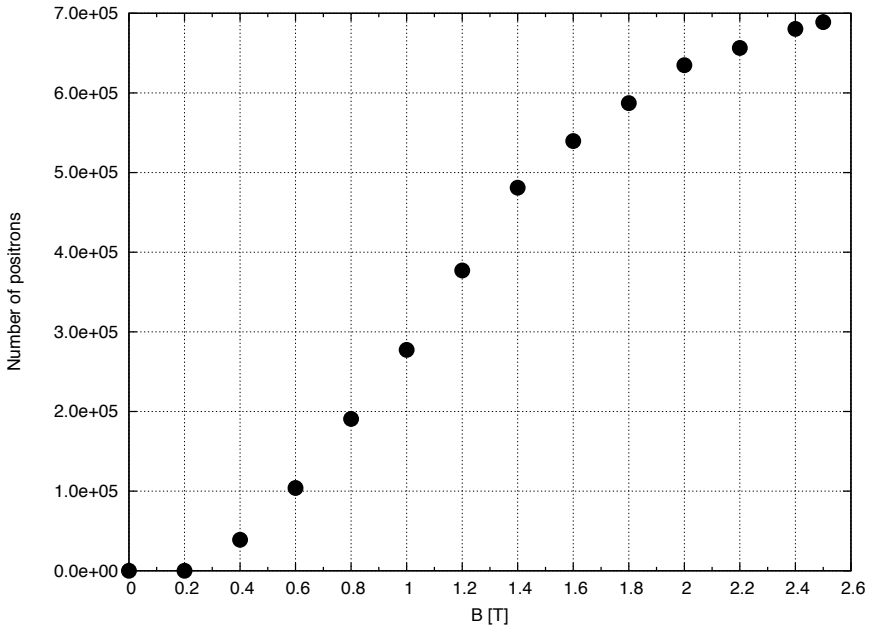

Figure 2.22: Magnetic field and the number of accumulated positrons. Accumulation time = 10 s, gas pressure = 9.8×10^{-2} Torr, bore temperture $\sim$ 100 K

2.5.2 Gas pressure

Gas pressure determines two competing factors which are related to the accumulation efficiency. One is the reaction rate of direct electronic excitation which is proportional to the gas density . The other factor is the life time of trapped positrons which is inversely proportional to the density. We found the optimized pressure for accumulating positrons at the bore temperature about 100 K. Figure 2.23 shows the relative number of positrons as a function of gas pressure measured by the vacuum gauge 1. (See Fig. 2.17) It is seemed that the peak value exists between 0.1 Torr and 0.12 Torr. In the following experiments, the gas pressure is fixed in this peak region.

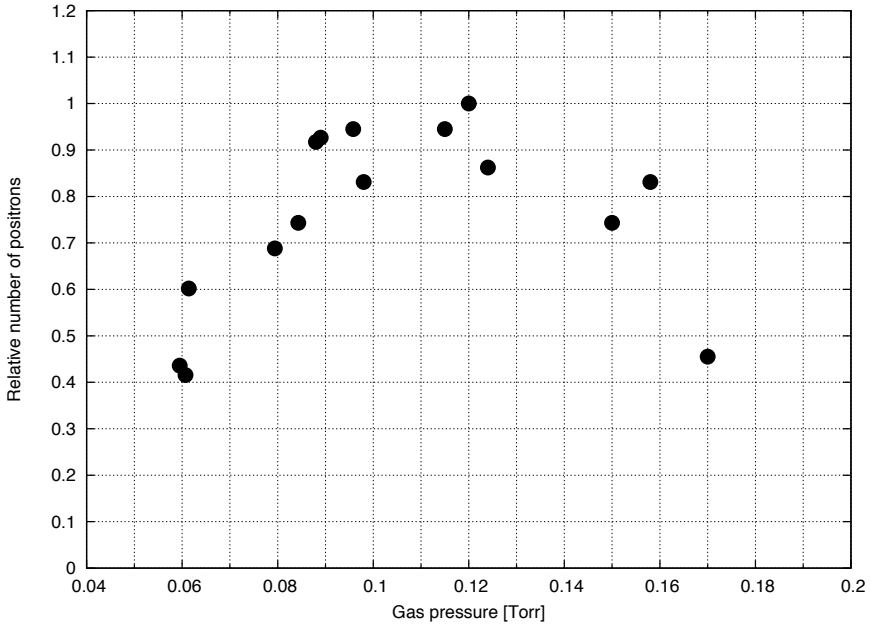

Figure 2.23: The relative number of accumulated positrons as a function of gas pressure. Accumulation time 10 s, B = 2.5 T, Bore temperature $\sim$ 100 K

2.5.3 Accumulation time

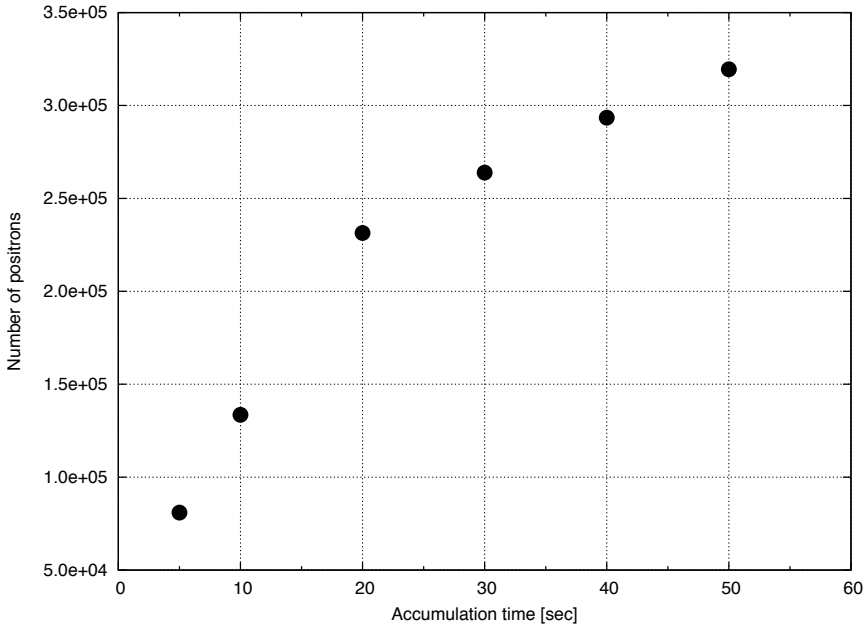

Figure 2.24: Accumulation time and the number of accumulated positrons. Gas pressure = 0.12 Torr, B = 2.5 T, Bore temperature $\sim$ 100 K

The number of positrons increases when the accumulation time is long although there is a limitation by annihilation.

Chapter 3

Transportation and trapping of positrons

Before being mixed with antiprotons, positrons must be transported to Cusp trap with a high transportation efficency. Since Cusp trap has the magnetic zero point at the center, radial expansoin causes the loss of charged antiparticles passing through the trap from one side to the other side. Therefore both of positron accumulator and antiproton trap are positioned in the same side of Cusp trap. According to this geometric limitation, transportation line is designed as seen in Fig. 3.1. The Green lines shows the trajectories of the positrons calculated by using CST studio (Computer Simulation Technology AG). In this calculation, 49 positrons setted 6 mm $\times$ 6 mm in the positron accumulator are ejected to the transportation line with 100 eV, assuming that the perpendicular energy of them are less than 1 eV. Figure 3.2 is a photo of the transportatin line.

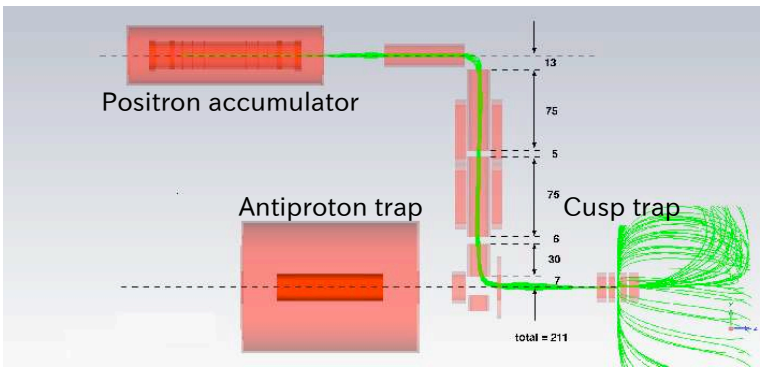

Figure 3.1: Transportation line

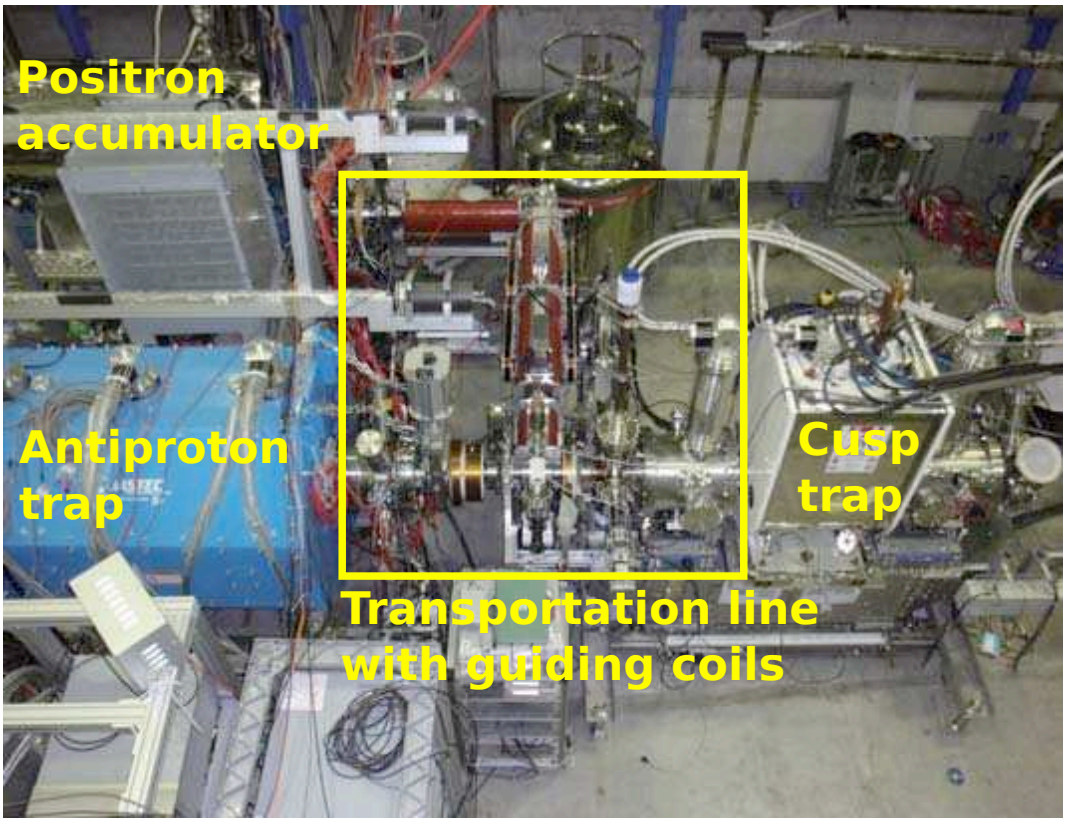

Figure 3.2: A photo of transportation line during installation.

3.1 Structure of trasportation line

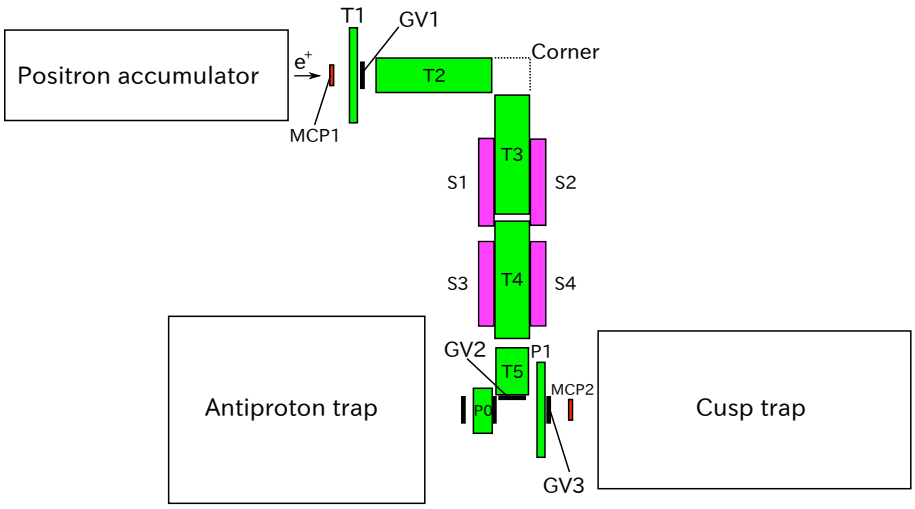

Figure 3.3: A brief view of transportation line

Figure 3.3 gives a brief view of transportation line. It consists of 7 guiding solenoid coils and 4 steering coils. Among them, T1, T2, T3, T4, T5, and P1 generate the magnetic fields to transport the positrons to Cusp trap. Concerning the magnetic field leakage from antiproton trap and Cusp trap, steering coils S1, S2, S3, S4 are equipped at the side of T3 and T4 to correct the trajectory of positrons. P0 is off when positrons are transported because it is only needed for antiproton transportation.

As mentioned in section 2.3.6, MCPs are used with phosphor screens for monitoring positrons extracted from the positron accumulator. For simplicity, combinations of them are named MCP1 and MCP2 respectively in Fig. 3.3. Through glass viewports installed nearby MCP1 and MCP2, the profile of positron beam is taken by CCD camera.

3.2 Test of transportating positrons

To check the loss of positrons and correct the trajectory, testing transportation of positrons is done step by step from positron accumulator to Cusp trap. If the trajectory of positron beam is away from the axis of the transportation line, some of them would be lost by collision with the wall of transport line. Especially at the corners, the radial size of positron increases because the magnetic flux expands.

Plastic scintillator is used for observing the annihilation of positrons when the beam hits the transportation line. The position of the annihilation is controlled by setting gate valves and guiding coils. Plastic scintillator is poistioned nearby this predicted point. In addition, for the energy of positron beam is known from the shape of extraction potential applied by MRE of the positron accumulator, arrival time to specific position is calculated. Therefore, if calculated time and observed time of arrival are the same, it could be concluded that some of positrons reached the predicted point. If not, detector would be moved forward position to determine the loss point. The signal of scintillator increases when it is close to the annihilation. The above method is applied repetitively as following steps.

	MCP1	GV1	GV2	GV3	MCP2	T1	T2	T3	T4	T5	P1
1	IN	IN	IN	IN	OUT	50A	0	0	0	0	0
2	OUT	OUT	IN	IN	OUT	50A	72A	0	0	0	0
3	OUT	OUT	IN	IN	OUT	50A	72A	72A	72A	90A	0
4	OUT	OUT	OUT	IN	OUT	50A	72A	72A	72A	90A	50A
5	OUT	OUT	OUT	OUT	IN	50A	72A	72A	72A	90A	50A

Figure 3.4 reveals the graph of arrival time at the several points. The slope of linear line is a reciprocal of positron velocity. Kinetic energy of a positron extracted from MCP1 is

$$\begin{aligned} \frac{1}{2}mv_{positron}^2 &= 0.5 \times (9.109 \times 10^{-31}kg) \times (\frac{1}{148} \times 10^9 m/s)^2 \\ &= 2.09 \times 10^{-17}J = 130eV \end{aligned} \tag{3.1}$$

This value is consistent with potential energy of bottom of accumulation well where positrons are trapped before extraction.

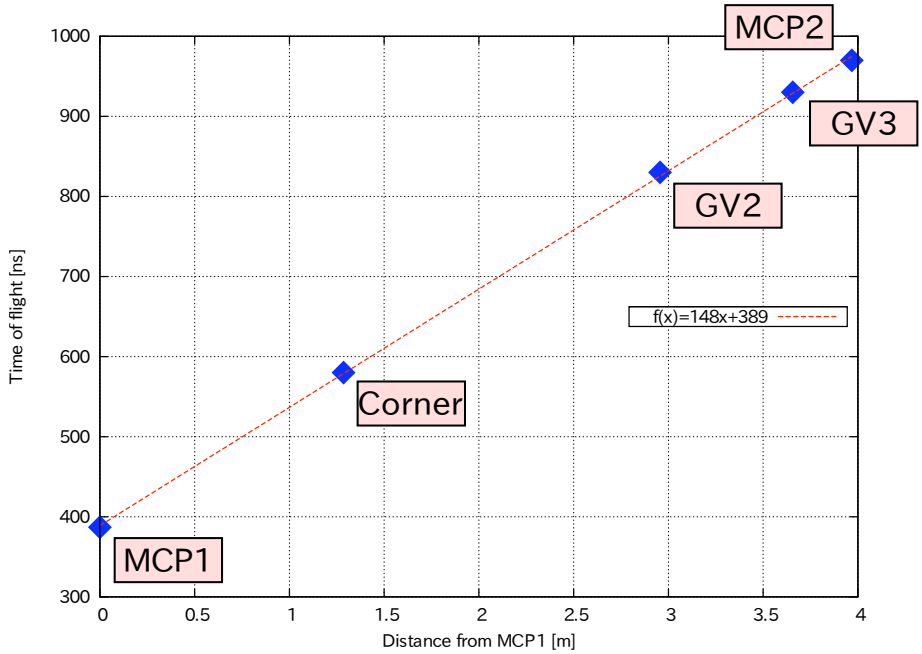

Figure 3.4: TOF of a positron beam as a function of the annihilation position. Red line is a linear funcition fitted to experiment data (blue diamonds).

Target	Distance [m]	Time [ns]
MCP1	0	0
Corner	1.29	390
GV2	2.96	580
GV3	3.66	830
MCP2	4.97	970

Table 3.1: The distance between the target and MCP1 and the arrival time of positrons.

Figure 3.5 shows a beam profile image taken by a CCD camera nearby MCP2. It seemed that some of positrons are lost when they are passing through the corner because the two sides of the beam are cut.

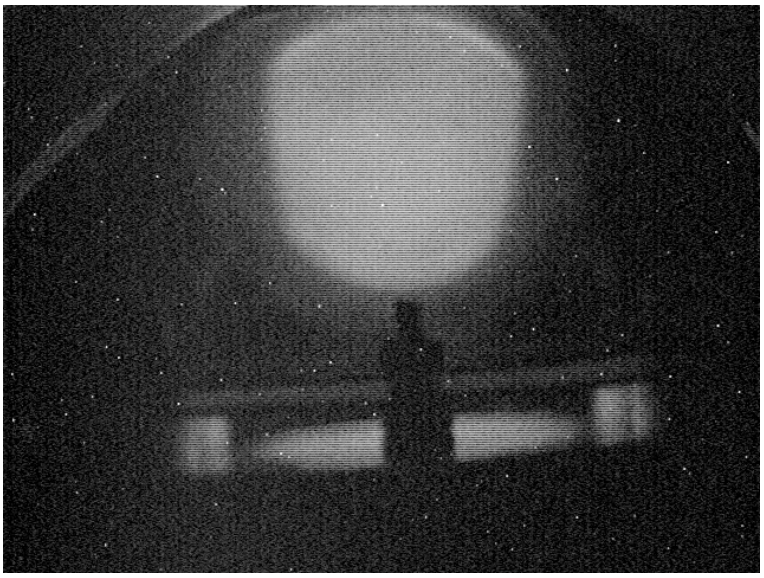

Figure 3.5: Beam profile of positrons at MCP2 (step 5)

3.3 Positron catching in Cusp trap

In this section, the process of positron catching will be described. A brief diagram of the process of transportation is shown in Figure 3.6. Firstly, electric potential for catching pulsed positron beam is prepared before positrons are extraced from the accumulator. When they are ejected by removing a potential barrier of the positron accumulator, one side of catching potential is decreased less than the energy of the positrons. Then positrons are transferred through transportation line and injected into Cusp trap. In order to confine the injected positrons, catching potential in Cusp trap returns to the original as first. Since the positrons are captured in the strong magnetic field, they lose their energy by synchrotron radiation. Eventually the positrons cool down to the environent temperature of the bore of Cusp trap.

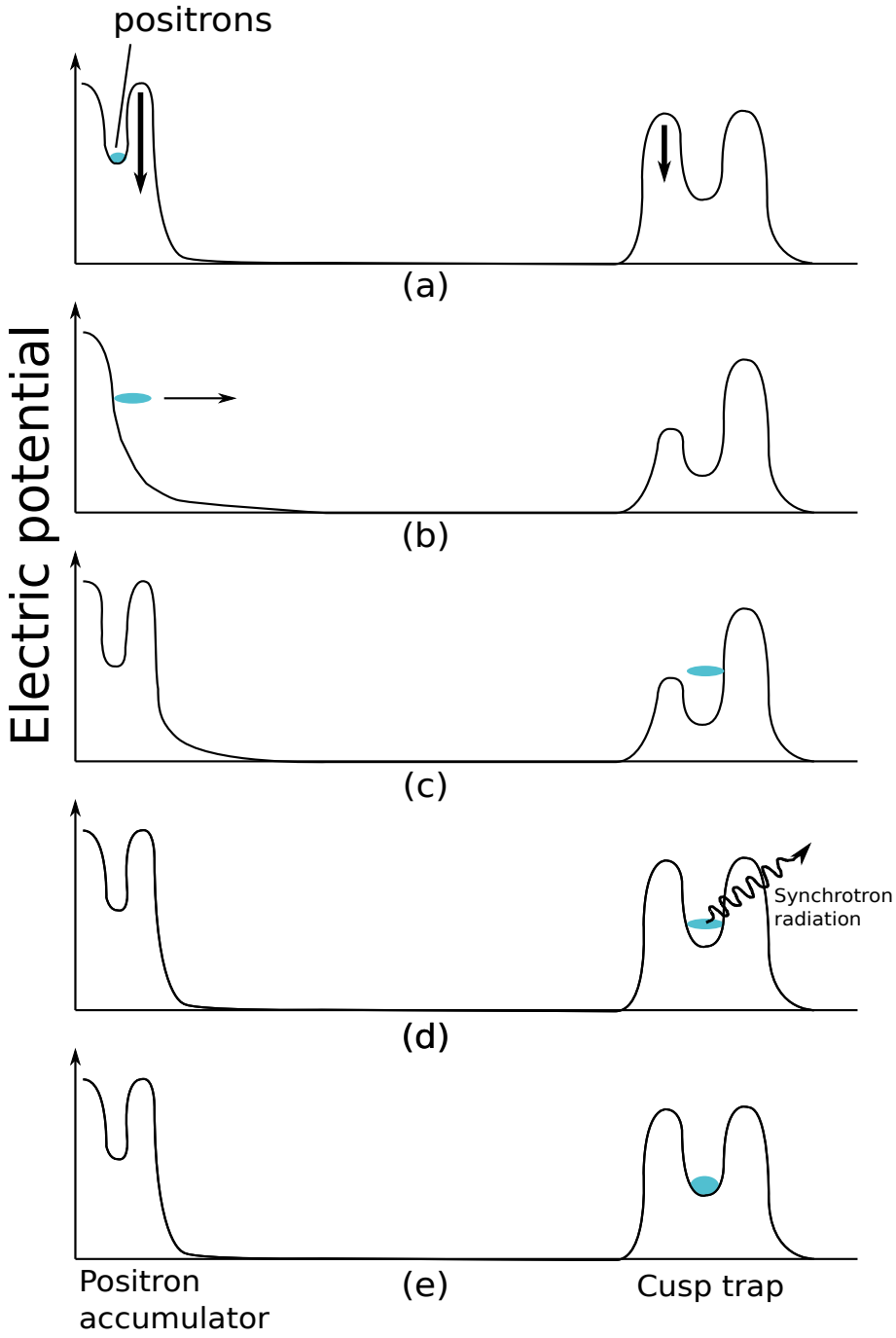

Figure 3.6: A diagram of the transporting process.

3.3.1 Catching potential

Figure 3.7 shows the potential for catching positrons. Purple line is the shape of potential during stand by. Potential barriers on both sides are set to 140 V and 175 V respectively. When positrons are injected to Cusp trap with kinetic energy about 130 eV, the barrier of upstream side is decreased to about 90 V as Red line. Then the barrier returns to 140 V again after positrons are in the trap.

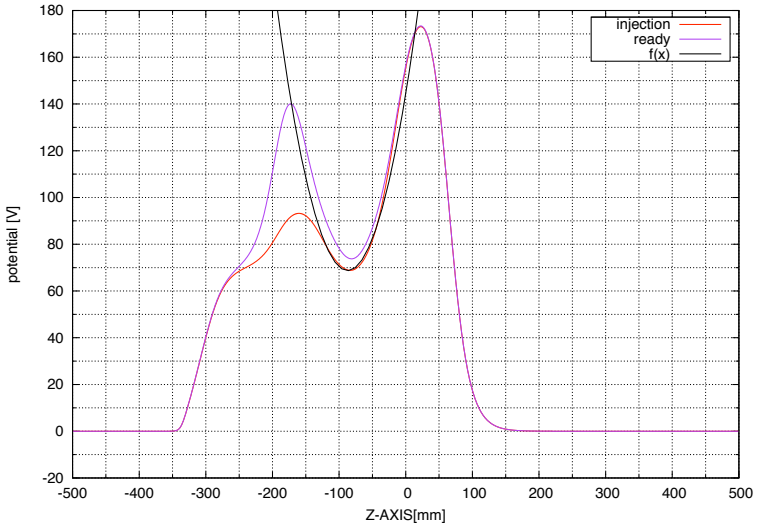

Figure 3.7: Catching potential

#	U9,8	U7	U6	U5	U4	U3	U2	U1	C	D1	D2	D3-D7
Ready	50	200	100	70	60	70	100	150	200	200	200	0
Injection	50	91	100	70	70	100	200	200	200	200	200	0

Table 3.2: Potential setting for catching positrons injected from upstream

f(x) is a harmonic function obtained by curve fitting to catching potential at the moment of injection. The fitting range is from -115 mm to -50 mm. If the center of f(x) is set up to the origin, it can be written as $f(z) = az^2 + b[V]$ where $a = 9.6 \times 10^4[V/m^2]$ and $b = 68.7[V]$. Then, the stay time of the positron beam in the catching potential can be estimated by solving the following proplem.

$$m_e \frac{d^2 z}{dt^2} = -2aqzt \tag{3.2}$$

where m_e is the mass of positron and q is the elementary charge. The periodic time of the oscilliation derived from the above equation is $2\pi\sqrt{\frac{m}{2aq}} \sim 140ns$.

3.3.2 Extraction for measuring the number of trapped positrons in Cusp trap

To check the transporting operation is in working order, the trapped positrons in Cusp trap are ejected again to the upstream side to be measured by MCP2. MCP2 is inserted into the axis with phosphor screen. Phosphor screen is used as a Faraday cup while MCP2 is amplifying the signal from positrons. This is the same situation of measuring the number of positrons extracted from positron accumulator. The profile of positron is also taken by using a CCD camera.

In addition, a plastic scintillator is laid on the fixed place close to MCP2. When the positrons collide with one side of MCP, they annihilate with radiating gamma rays whose number is proportional to the number of annihilated positrons. Then some of these gamma rays hit the plastic scintillator. Since the solid angle of the scintillator is constant, the relative value of the amount of positrons is inferred by comparing the signal from each operation of positron extraction. The absolute number of positrons can also be earned by comparing between the signals of MCP2 and the scintillator first.

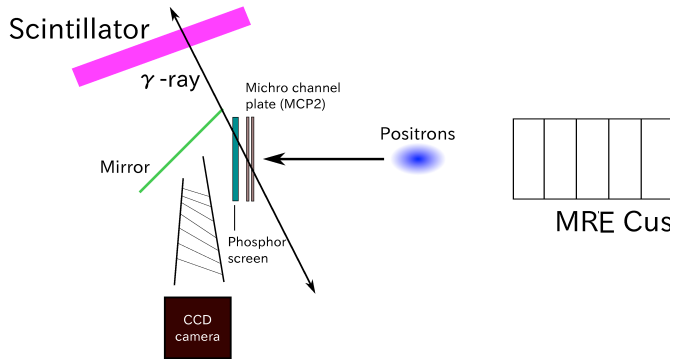

Figure 3.8: A schematic view of the monitor system (MCP2)

Figure 3.9 shows the potential manipulation to extract the positrons trapped in the catching potential.

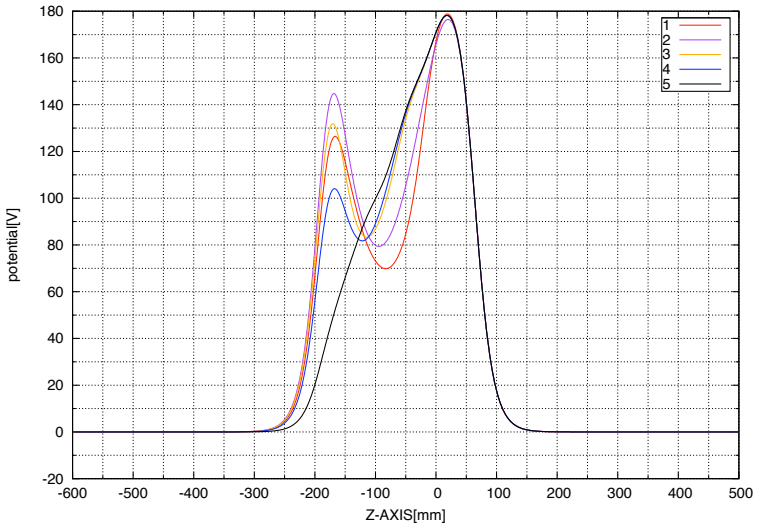

Figure 3.9: Manipulation from catching potential to extraction potential

#	U9,8	U7	U6	U5	U4	U3	U2	U1	C	D1	D2	D3	D4-D7
1	50	200	100	70	60	70	100	150	200	200	200	200	0
2	50	200	100	70	70	100	200	200	200	200	200	200	0
3	50	200	135	90	135	150	200	200	200	200	200	200	0
4	0	200	135	90	135	150	200	200	200	200	200	200	0
5	0	200	26	90	135	150	200	200	200	200	200	200	0

Table 3.3: Potential settings for manipulation from catching to extraction

3.3.3 Timing of catching positron

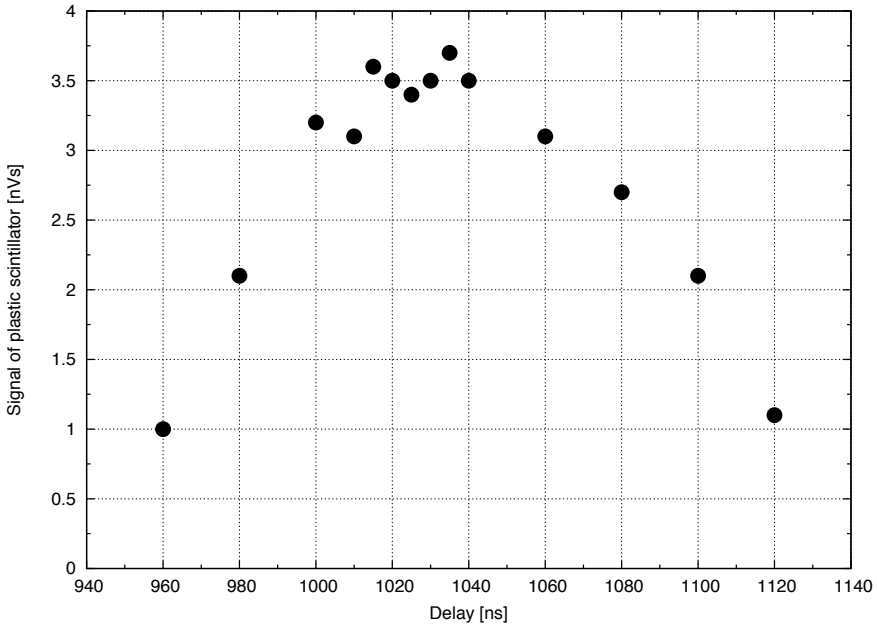

Figure 3.10: Delay and signal from plastic scintillator

Figure 3.10 shows the relation between the time setting of delay and trapped positrons. The distance from MCP2 to the center of catching potential is 730 mm. As derived from section 3.2, the velocity of the positron beam is $6.8 \times 10^6 m/s$. Therefore it is estimated that the beam reaches the center of catching potential 1070 ns after passing through the position of MCP2. It seemed the peak region is shifted because of rising time of the potential barrier, which is about 50 ns.

3.3.4 Positron lifetime in catching potential

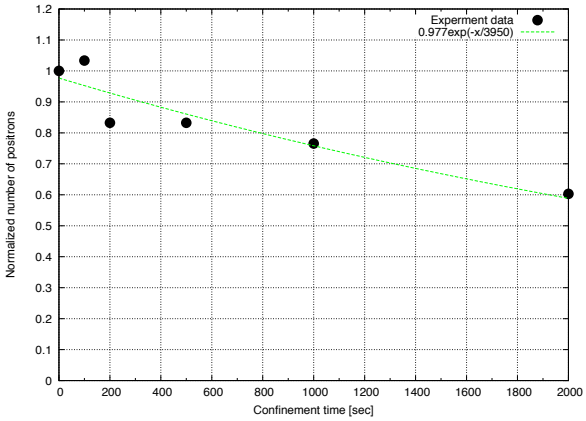

Figure 3.11: Time evolution of the number of positrons in catching potential (Measured by MCP)

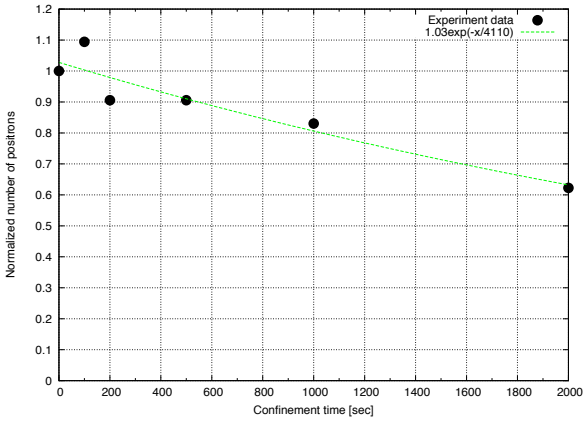

Figure 3.12: Time evolution of the number of positrons in catching potential (Measured by plastic scintillator)

Figure 3.11 and Figure 3.12 show the time evolution of the normalized number of positrons. The horizontal axis reveals the passed time after catching operation and the vertical axis represesnts the normalized number of the extracted positrons. As mentioned above, positrons are observed by MCP2 and plastic scintillator when they collide with MCP2 and emmit gamma rays produced by annihilation.

3.4 Stacking operation

It is expected that more than a million of positrons are needed to synthesize antihydogens enough to be detected. Therefore we increase the number of positrons in Cusp trap by overlapping multiple injections. This is possible because positrons injected into the trap lose their energy by sychrotron radiation. If there is a enough time interval between operations, the priorly trapped positrons cannot escape even when the barrier is lowered for the next injection. After the injection of additional positrons, potential barrier returns to the original level immediately so they can be added to prior ones. This procedure is called stacking operation.

In addition, these additionally injeceted positrons lose their energy by colliding with priorly trapped ones, which have been cooled down to the environment temperature of the bore of Cusp trap. Simultaneously, positrons taking energy from the collision radiate their energy by synchrotron radiation. Finally the state of positrons reaches equillibrium which doesn't allow any escape of positrons.

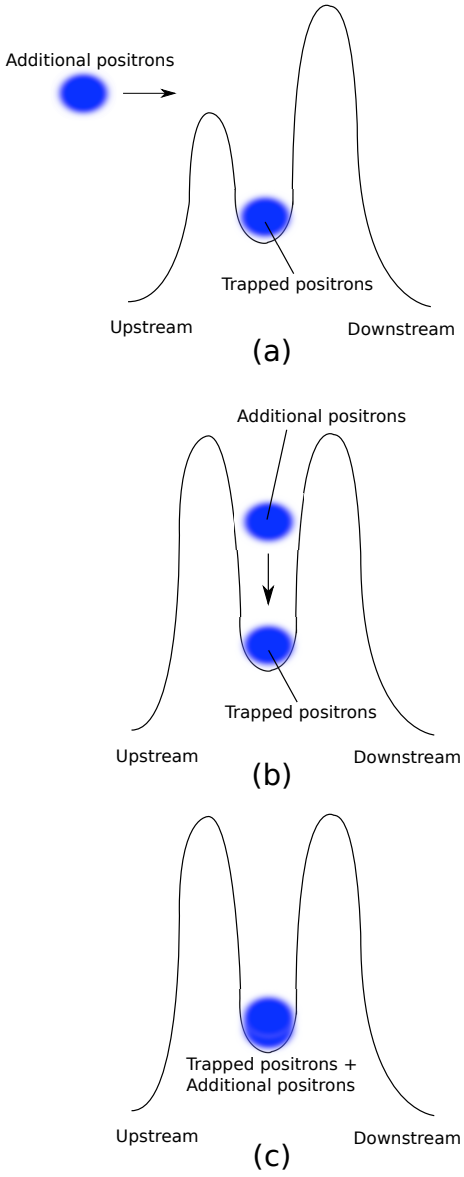

Figure 3.13: A diagram of the stacking process. Positrons are caught into Cusp trap gradually. Priorly trapped positrons have lost their energy before new positrons are injected. (a) Additional positrons are injected to the trap. (b) Potential barrier is increased. Prior positrons are heated by colliding with new positrons and losing their energy by synchrotron radiation. This cooldown process is recurred until (c) the state of positron cloud reaches equilibrium

Figure 3.14 and Figure 3.15 show that the number of positrons increases when the stacking process is in operation. Data points of Fig. 3.14 are measured by MCP2 using the front of the MCP as a Faraday cup. As is seen in these two graphs, signal from the plastic scintillator is proportional to the number of positrons which hit the MCP. Measured by the plastic scintillator, 1 nVs signal corresponds to 5×10^4 positrons.

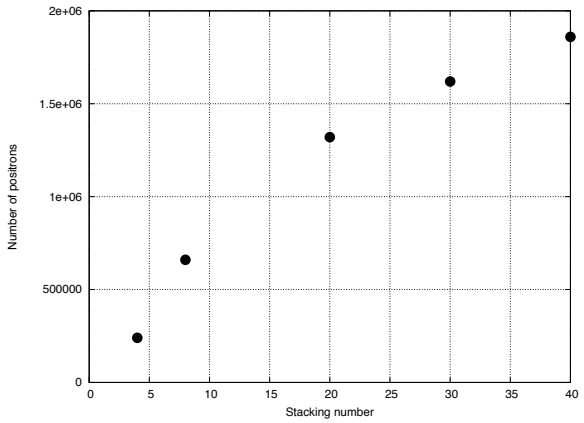

Figure 3.14: The number of trapped positrons increases when the stack number is bigger (measured by MCP)

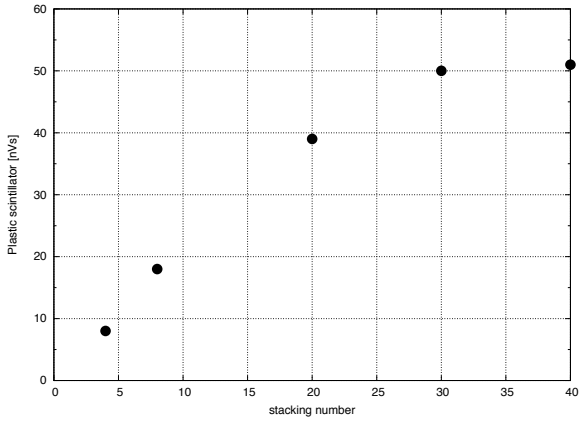

Figure 3.15: The number of positrons increases when the stack number is bigger (measured by plastic scintillator)

Chapter 4

Positron manipulation in Cusp and antihydrogen synthesis

4.1 Scheme of antihydrogen synthesis

Figure 4.1 gives the procedure of antihydrogen synthesis in Cusp trap. (a) As mentioned in chapter 3, positrons are trapped by the stacking operation. (b) To mix trapped positrons and antiprotons, potential shape is changed from catching potential to nested potential. (c) Antiprotons are injected from antiproton trap while upstream barrier of nested potential is decreased. (d) Potential barrier returns to the same level of (c) immediately after antiprotons come into the nested trap.

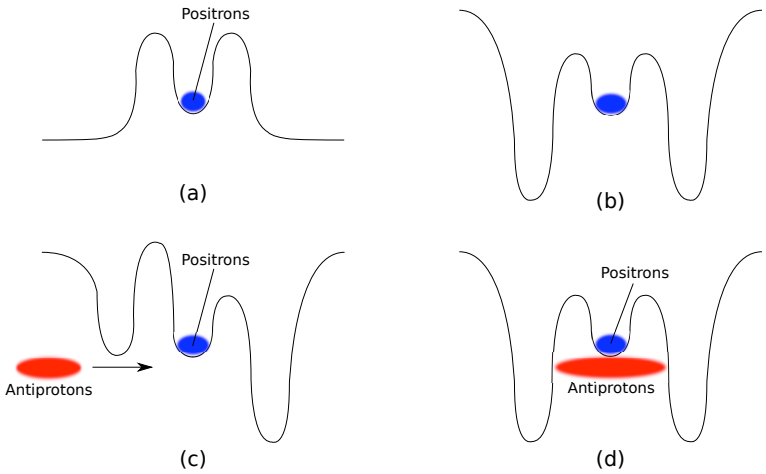

Figure 4.1: A brief scheme of antihydrogen synthesis

4.2 Radial compression by rotating wall method

The density of positron cloud is one of the important factors to effectively synthesize antihydrogen atoms. The recombination rate of them increase when the positron cloud has a high density. For this purpose, positron cloud trapped in Cusp trap is radially compressed by applying rotating electric field of U4 (See Fig. 1.6) during the stacking operation. As is seen in Fig. 4.2 (a), the electrode U4 is segmented into four. By applying sinusoidal wave to each separated electrode of the ring, the rotating field is provided as shown in Fig. 4.2 (b).

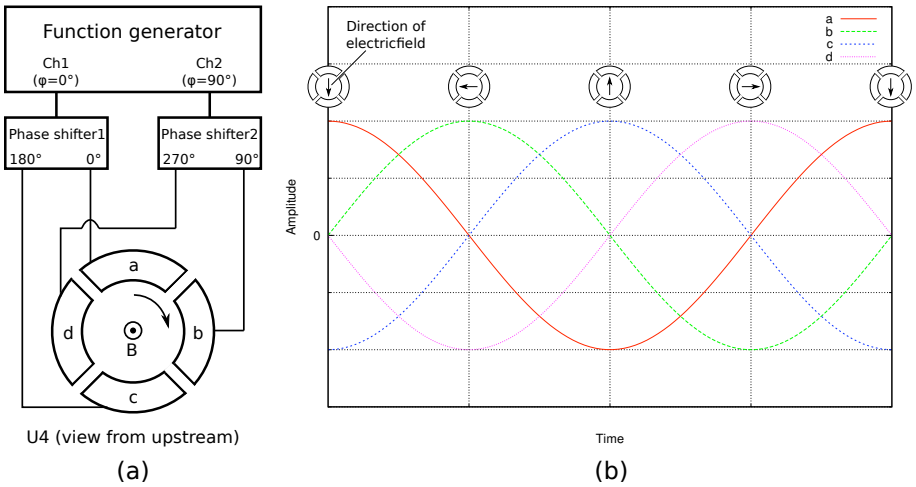

Figure 4.2: (a) A combination of a function generator and two phase shifters provides four oscillating potentials given by $A\sin(kx-\omega t+\phi_i)$, where $\phi_i = \frac{\phi}{2}i$. (b) Phase difference between neighboring parts is 90°. Electrode a is the fastest. Then b, c, and d are followed in order. This order determines the direction of rotating field which corresponds to the rotation direction of positron cloud.

Figure 4.3 (a) and Figure 4.3 (b) show the phosphor scree images of positron clouds extracted from Cusp trap after 20 stacks. Figure 4.3 (a) is obtained when the positron cloud is radially compressed by applying a rotating field during the stacking operation. The amplitude of the rotating field is 10 V while its frequency is swept from 13 MHz to 14 MHz during 1000 s. In the case of Fig. 4.3 (b), positron cloud spreads over the region of the phosphor screen.

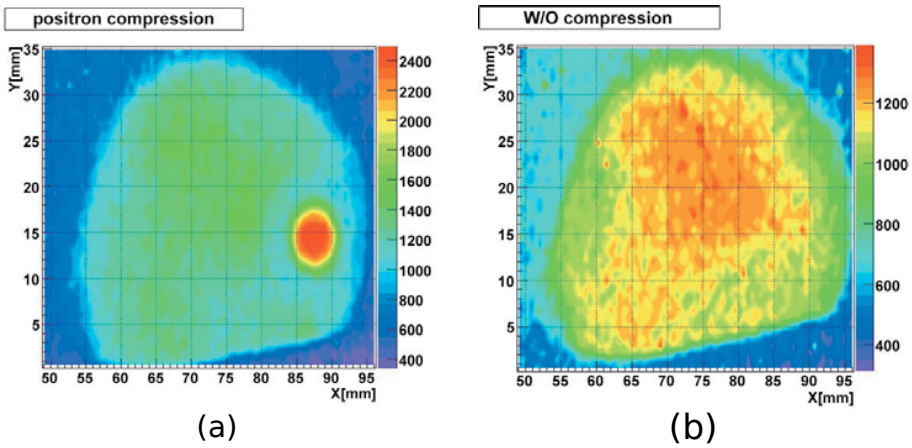

Figure 4.3: Phosphor screen images of positrons extracted from Cusp trap (a) with radiall compression and (b) without radial compression.

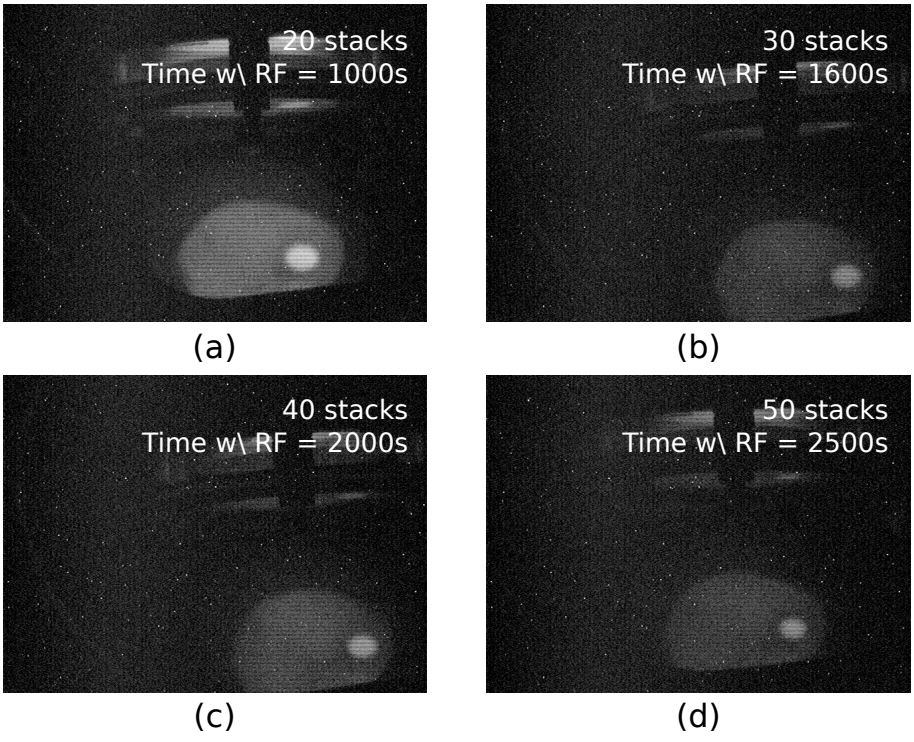

Figure 4.4: The radial size of positron cloud decreases when rotating field was applied longer

As is seen in Fig. 4.4, the radial size of positron cloud is smaller when the stacking time with rotating field is longer. The bright circle in the image implies compressed positrons while the not compressed component ones collide with other region of phsphor screen which emmits a vague light.

Figure 4.5 shows the number of positrons accumulated in Cusp trap increases linearly up to 6×10^6 when the positron cloud is compressed during the stacking operation. It is inferred that the positron life time with radial compression is several times longer than the case without radial compression.

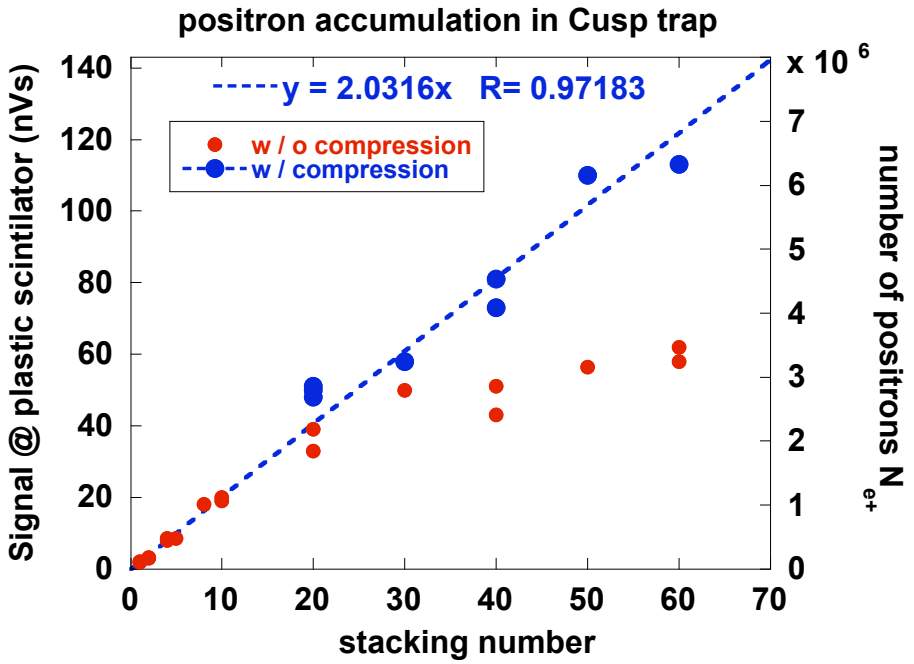

Figure 4.5: The number of positorns extracted from Cusp trap with (blue circles) and without (red circles) radial compression.

4.3 Potential manipulation from catching potential to nested potential

After the stacking operation with the radial compression, potential is changed to the nested trap to mix positrons with antiprotons . To keep the trapped positrons cold in the trap, this manipulation was made smoothly and quietly. (See Fig. 4.6)

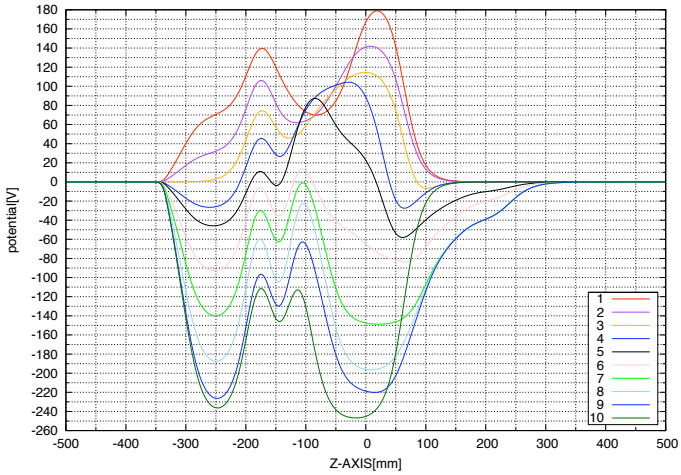

Figure 4.6: Manipulatoin from catching potential to nested potential

#	U9,8	U7	U6	U5	U4	U3	U2	U1	C	D1	D2	D3	D4	D5	D6	D7
1	70	200	100	70	60	70	100	200	200	200	200	200	0	0	0	0
2	30	180	40	60	60	100	150	150	150	150	150	150	0	0	0	0
3	0	140	20	40	80	100	120	120	120	120	120	120	-50	0	0	0
4	-30	120	-40	80	100	100	120	120	100	100	100	-80	-20	0	0	0
5	-50	80	-90	100	120	40	40	40	30	30	30	-100	-50	-30	-20	-10
6	-100	-100	100	-150	100	-30	-50	-50	-50	-80	-80	-80	-100	-50	-40	-20
7	-150	100	-200	100	-30	-150	-150	-150	-150	-150	-150	-150	-150	-80	-60	-40
8	-200	100	-280	100	-50	-200	-200	-200	-200	-200	-200	-200	-150	-80	-60	-40
9	-240	50	-280	50	-100	-220	-220	-220	-220	-220	-230	-230	-150	-80	-60	-40
10	-250	28	-280	25	-250	-250	-250	-250	-250	-250	-250	-250	0	0	0	0

Table 4.1: Potential settings from catching potential to nested potential

4.3.1 Positron lifetime in the nested potential

The positron life time in the nested potential is measured by extraction with changing confinement time. As is seen in Figure 4.7 and Figure 4.8, the 1/e life time is about 3000 s. This life time is long enough to mix positrons with antiprotons altough it is 1000 s short compared to the case of the catching potential.

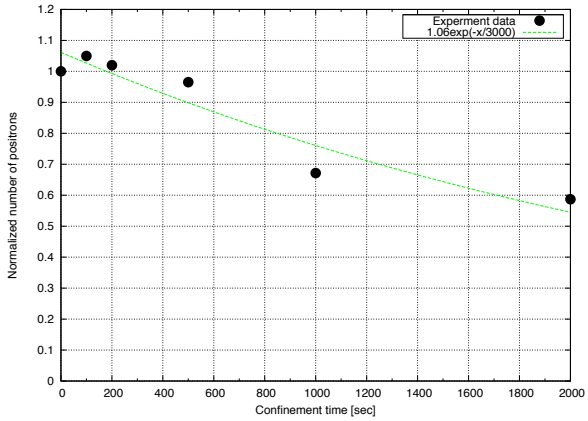

Figure 4.7: Time evolution of the number of positrons confined in the nested potential (measured by MCP)

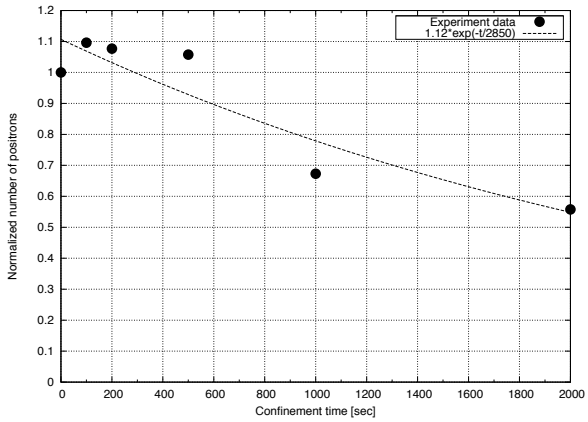

Figure 4.8: Time evolution of the number of positrons confined in the nested potential (measured by plastic scintillator)

4.3.2 Time evolution of the profile of positrons

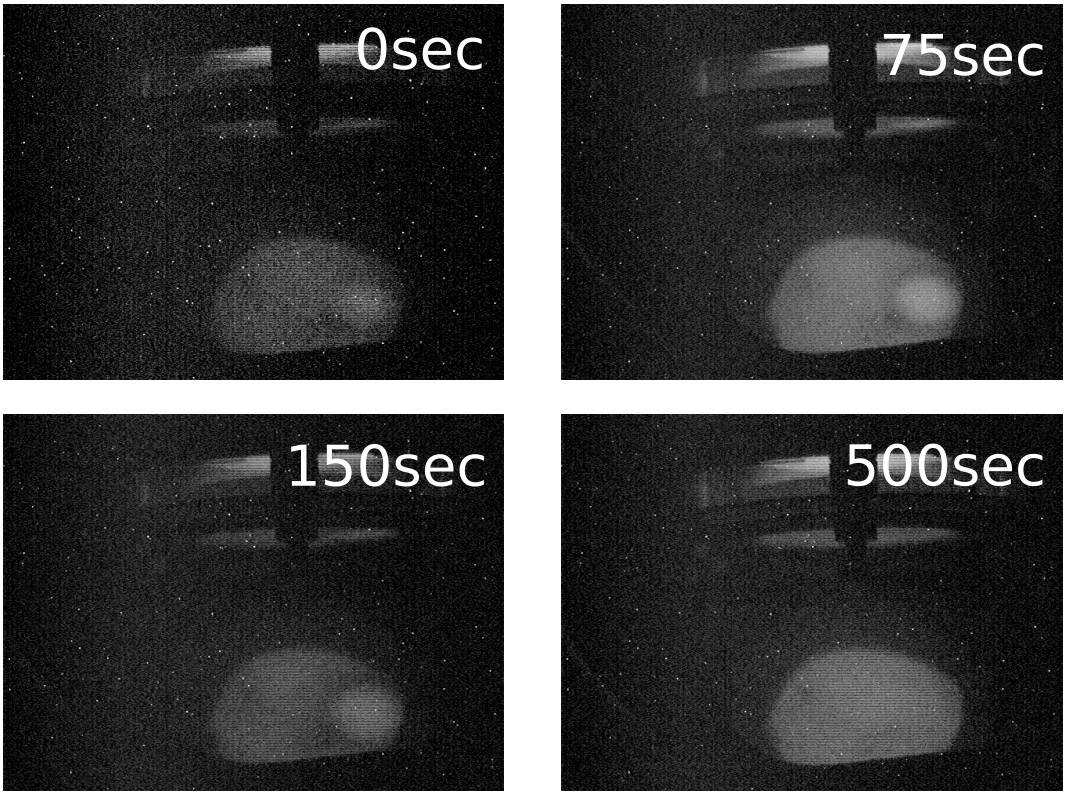

Figure 4.9: Time evolution of positron beam profile (stacking number = 20)

Figure 4.9 shows variations of the profile of positron cloud in nested potential spreads radially with the passing of time. It is observed that radial size of positron cloud grows during the confinement time.

4.4 Antihydrogen synthesis

4.4.1 Antiproton injection

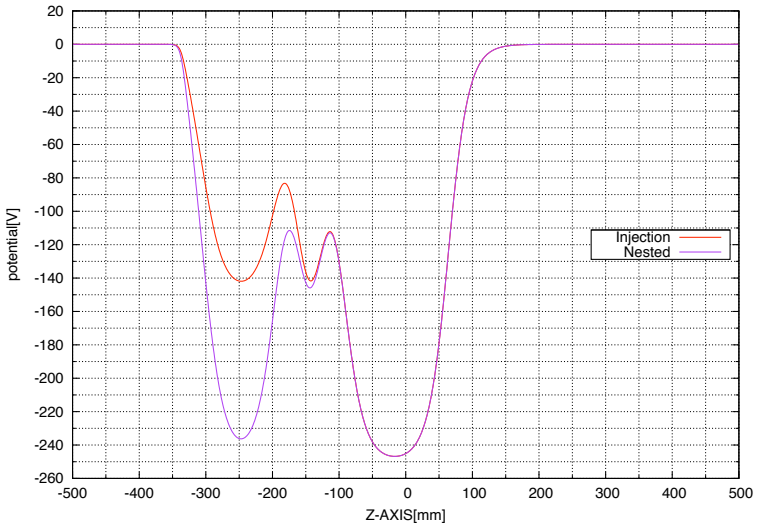

Figure 4.10: Potential configuration for injecting antiprotons

#	U9,8	U7	U6	U5	U4	U3	U2	U1	C	D1	D2	D3	D4-D7
Nested	-250	28	-280	25	-250	-250	-250	-250	-250	-250	-250	-250	0
Injection	-250	28	-280	25	-250	-250	-250	-250	-250	-250	-250	-250	0

Table 4.2: Potential setting for antiproton injection

The method of catching antiprotons is the same as catching positrons while the sign of the potential barrier is the opposite. The potential barrer of the upstream side is removed before antiprotons are injected. Then it returns immediately after antiprotons get into the potential. (See Fig. 4.10)

4.4.2 Field Ionization

To detect the antihydrogens formed in the nested potential, so-called field ionization method is used. Figure 4.11 is a schematic illustration of this method. The procedure to detect antihydrogen atoms consists of following steps.

(a) Antihydrogens are formed in the region where antiprotons overlap positrons.

(b) Since the antihydrogens are electrically neutral, they spread isotropically. Field ionization well is prepared at the downstream of Cusp trap.

(c) Some of antiprotons are reached to the field ionization well. If the antihydrogens are in high Rydberg states, they are eventually ionized and their antiprotons are accumulated in the well.

(d) Antiprotons accumulated in the field ionization well are dumped to the downstream. They spread along the magnetic field lines, hit some part of the apparatus and annihilate. If annihilations of the antiprotons are detected at the moment, it means that antihydrogens were synthesized.

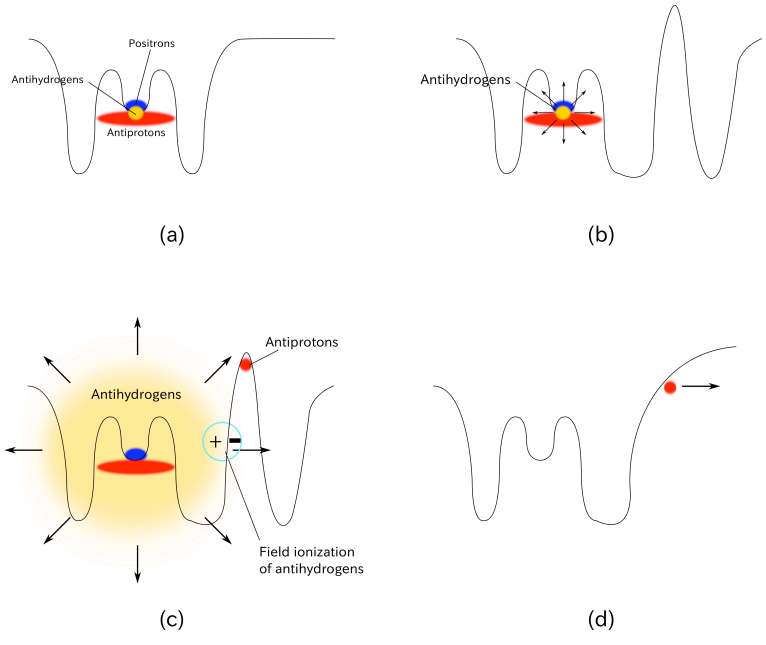

Figure 4.11: Procedure of field ionization

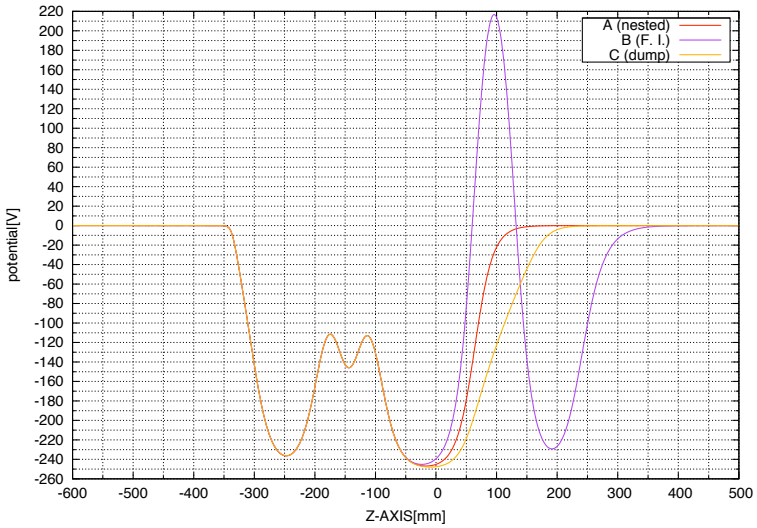

Figure 4.12: Potential manipulatoin for field ionization

#	U9,8	U7	U6	U5	U4	U3	U2	U1	C	D1	D2	D3	D4	D5	D6	D7
nested	-250	28	-280	25	-250	-250	-250	-250	-250	-250	-250	-250	0	0	0	0
F. I	-250	28	-280	25	-250	-250	-250	-250	-250	-250	-250	-250	350	350	-250	-250
dump	-250	28	-280	25	-250	-250	-250	-250	-250	-250	-250	-250	-150	-100	-50	0

Table 4.3: Potential setting for field ionization

Figure 4.11 shows potentials performed for field ionizations. We excecute combinations of them as following order.

$$A \rightarrow [B \rightarrow wait\ 5s \rightarrow C \rightarrow wait\ 0.1s]$$

After the antiproton injection, nested potential A is immediately changed to B, which has a field ionization well at the downstream side. As described in Fig. 4.11, if antihydrogens are formed and freed from the nested potential, some of them reaches the field ionization well and then their antiprotons are eventually trapped in the well. To accumulate the antiprotons, the manipulation stops for 5 s. Then accumulated antiprotons in the field ionization well are ejected to the downstream. These accumulating and ejecting processes revealed in the square bracket are repeated for 20 times.

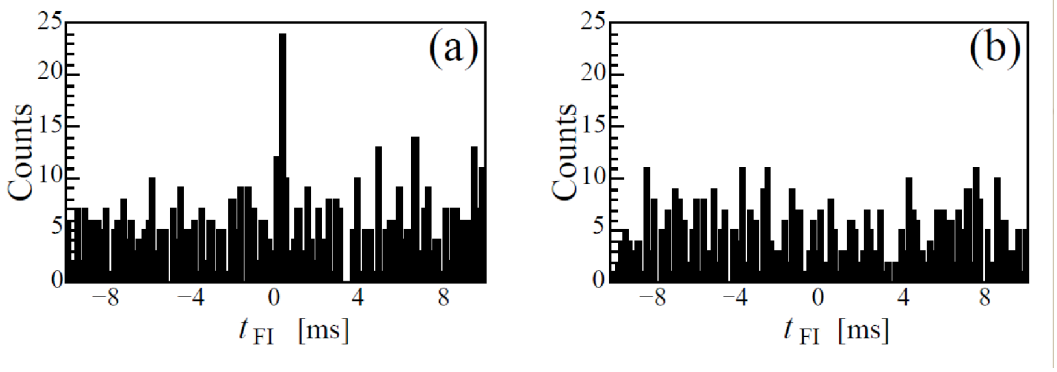

Figure 4.13: The time spectra obtained by summing the spectra around the the timing of the first ten field ionization well openings ($-10ms < t_{FI} < 10ms$) (a) with and (b) without positrons.

Figure 4.13 shows the counts from 3D detector during the mixing of antiprotons with (a) and (b) without positrons. $t_{FI} = 0$ is the timing when the field ionization well is collapsed. As is seen, a sharp peak appeared at the timing $t_{FI} = 0$ only if positrons are trapped in the nested potential, which means antihydrogens are field-ionized and their antiprotons are accumulated in the field ionization well. The backgrounds are mainly due to the annihilation of trapped antiprotons or cosmic rays.

Chapter 5

Summary

As important ingredient for synthesizing antihydrogen atoms, positrons were succesfully accumulated in the trap using the buffer gas method. 2.5×10^5 positrons were accumulated during 30 s. Parameters including gas pressure, magnetic field, and temperature of the inner bore of the trap were optimized to increase the accumulating efficiency. Potential configuration for accumulating positrons was the most hardly determined factor.

Transporting positrons from the positron accumulator to Cusp trap was done with about 50% efficiency. Typically, 1.5×10^5 positrons are succesfully captured by catching potential generated in Cusp trap. After transportation, positrons are radially compressed by applying rotating electric field to the side of catching potential during the stacking operation.

Manipulating positrons in Cusp trap was quickly and smoothly done. Immediately after stacking operation, potential configuration is varied smoothly from the catching potential to the nested potential. It was noted that positron cloud was still radially compressed after the potential manipulation from catching potential to the nested potential. The positron lifetime in the nested potential is about 3000 s which is enough to mix positrons with antiprotons. Mixing with antiprotons in the nested potential was succesfully done. Using field ionization method, antihydrogen atoms are detected by the 3D track detector.

Biblography

[1] B. Schwingenheuer, R.A. Briere, A.R. Barker, E. Cheu, L.K. Gibbons, D.A. Harris, G. Makoff, K.S. McFarland, A. Roodman, Y.W. Wah, et al. CPT Tests in the Neutral Kaon System. Physical Review Letters, 74(22):4376-4379, 1995.

[2] W.M. Yao, et. al. Review of Particle Physics. Journal of Physics G, 33:1, 2006.

[3] A. Mohri and Y. Y, Yamazaki, Europhys. Lett. 63, 207 (2003)

[4] E. Widmann, R.S Hayano, M. Hori, Y, Yamazaki. Nuclear Instruments and Methods in Physics Research B 214 (2004) 31-34

[5] J.M.B. Kellogg, I.I. Rabi, and J.R. Zacharias. The Gyromagnetic Properties of the Hydrogens. Physical Review, 50(5):472-481, 1936.

[6] I.I. Rabi, J.M.B. Kellogg, and J.R. Zacharias. The Magnetic Moment of the Proton. Physical Review, 46(3):157-163, 1934.

[7] J.E. Nafe and E.B. Nelson. The Hyperfine Structure of Hydrogen and Deuterium. Physical Review, 73(7):718-728, 1948.

[8] A.G. Prodell and P. Kusch. The Hyperfine Structure of Hydrogen and Deuterium. Physical Review, 79(6):1009-1010, 1950.

[9] G. Budker and A.N. Skrinsky. Electron cooling and new possibilities in elementary particle physics. Sov. Phys. -Usp., 21(4):277, April 1978.

[10] M.H. Holtzscheiter and M. Charlton. Ultra-low energy antihydrogen. Rep. Prog. Phys., 62(1):1, January 1999.

[11] G. Gabrielse, S.L. Rolston, L. Haarsma, and W. Kells. ANTIHYDROGEN PRODUCTION USING TRAPPED PLASMAS. Phys. Lett. A, 129(1):38, May 1988.

[12] G. Bauer, G. Boero, S. Brauksiepe, A. Buzzo, W. Eyrich, R. Geyer, D. Grzonka, J. Hauffe, K. Kilian, M. LoVetere, M. Macri, M. Moosburger, R. Nellen, W. Oelert, S. Passaggio, A. Pozzo, K. Rohrich, K. Sachs, G. Schepers, T. Sefzick, R.S. Simon, R. Stratmann, F. Stinzing, and M. Wolke. Production of antihydrogen. Phys. Lett. B, 368(1-3):251, February 1996.

[13] G. Blanford, D.C. Christian, K. Gollwitzer, M. Mandelkern, C.T. Munger, J. Schultz, and G. Zioulas. Observation of Atomic Antihydrogen. Phys. Rev. Lett., 80(14):3037, April 1998.

[14] M. Amoretti et al. Production and detection of cold antihydrogen atoms. Nature, 419:456, 2002.

[15] G. Gabrielse, N.S. Bowden, P. Oxley, A. Speck, C.H. Storry, J.N. Tan, M. Wessels, D. Grzonka, W. Oelert, G. Schepers, et al. Background-Free Observation of Cold Antihydrogen with Field-Ionization Analysis of Its States. Physical Review, 89(21):213401, 2002.

[16] N. Kuroda, H.A. Torii, K.Y. Franzen, Z.Wang, S. Yoneda, M. Inoue, M. Hori, B. Juhász, D. Horváth, H. Higaki, et al. Confinement of a Large Number of Antiprotons and Production of an Ultraslow Antiproton Beam. Physical Review, 94(2):23401, 2005.

[17] Murphy, TJ. ,Surko, CM. ,et al. Physical Review A. 46,5696-5705(1992)

[18] Oshima, N. ,Kojima, TM. ,et al. Physical Review B. 31,4123-4130(1985)

[19] Schultz, P.J. ,Lynn, KG. ,et al. Reviews of Modern Physics. 60,701-779(1988)

[20] J. P. Marler and C. M. Surko. Positron-impact ionization, positronium formation, and electronic excitation cross sections for diatomic molecules. Physical Review A 72, 062713, 2005.

[21] M. Charlton and J. Humberston, Positron Physics Cambridge University Press, New York, 2001 .